

~~CONFIDENTIAL FILE COPY~~

AFWAL-TR-80-4085

ADA093820



Determination of Crosslinking in High T_g Polymers

Research Triangle Institute
P. O. Box 12194
Research Triangle Park, N. C. 27709

July 1980

Final Technical Report AFWAL-TR-80-4085
15 October 1977 - 15 October 1979

Approved for public release; distribution unlimited

MATERIALS LABORATORY
AIR FORCE WRIGHT AERONAUTICAL LABORATORIES
AIR FORCE SYSTEMS COMMAND
WRIGHT-PATTERSON AIR FORCE BASE, OHIO 45433

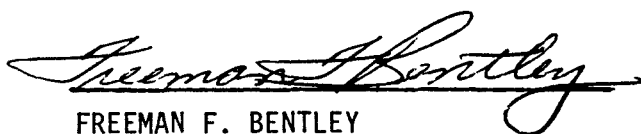
Best Available Copy 20040223010

NOTICE

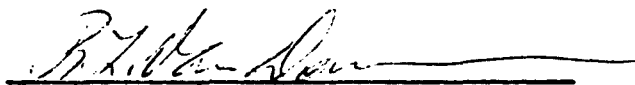
When Government drawings, specifications, or other data are used for any purpose other than in connection with a definitely related Government procurement operation, the United States Government thereby incurs no responsibility nor any obligation whatsoever; and the fact that the government may have formulated, furnished, or in any way supplied the said drawings, specifications, or other data, is not to be regarded by implication or otherwise as in any manner licensing the holder or any other person or corporation, or conveying any rights or permission to manufacture, use, or sell any patented invention that may in any way be related thereto.

This report has been reviewed by the Office of Public Affairs (ASD/PA) and is releasable to the National Technical Information Service (NTIS). At NTIS, it will be available to the general public, including foreign nations.

This technical report has been reviewed and is approved for publication.



FREEMAN F. BENTLEY
Project Engineer
Polymer Branch



R. L. VAN DEUSEN
Chief, Polymer Branch
Nonmetallic Materials Division

FOR THE COMMANDER



F. D. CHERRY, Chief
Nonmetallic Materials Division

"If your address has changed, if you wish to be removed from our mailing list, or if the addressee is no longer employed by your organization please notify AFWAL/MLBP, W-PAFB, OH 45433 to help us maintain a current mailing list".

Copies of this report should not be returned unless return is required by security considerations, contractual obligations, or notice on a specific document.

(continuation of block 20)

Most of the evidence for nodule formation in cured epoxy resins is derived from electron microscopic investigations of fracture surfaces by replication technique. Generally, the micrographs reveal the presence of globular domains with dimensions in the range of 10-70 nm. So far the existence of nodular structures could not be confirmed by x-ray scattering experiments. In view of the accumulated evidence for the presence of globular network inhomogeneities the lack of x-ray evidence would indicate an extremely small difference between the electron densities of nodules and imbedding matrix material. As a consequence the evaluation of x-ray particle scattering becomes experimentally rather demanding.

An attempt has been made to detect network inhomogeneities in crosslinked epoxy systems by means of small angle x-ray scattering. The SAXS intensity distribution consists of 1) a constant asymptotic value for a portion of the scattering curve, 2) a portion at larger scattering angles where scattering intensity increases gradually with increasing scattering angle and 3) a portion at very small angles where the intensity increases markedly with decreasing scattering angle. Portion 1 of the scattering curve is ascribed to density fluctuations within regions of relatively constant density in the material and is a constant term independent of scattering angle. Portion 2 is the tail of the wide-angle x-ray scattering. Portion 3 has been found in many studies of amorphous systems in general and of epoxy systems in particular and is ascribed to heterogeneities in the system. Although this portion was of very low scattering power, it was chosen for further study because the low room temperature density difference between cured and uncured epoxy systems would be consistent with a scattering curve of such low scattering power caused by nodules of highly crosslinked resin in a less highly crosslinked matrix. No systematic variation of scattering power or correlation distance (derived from an analysis of portion 3 of the scattering curve) was found with increasing curing temperature for three cured epoxy systems. Portion 3 appears to originate at the film surface and to be associated with the release agent (Frekote) applied to the glass plates between which curing was carried out. A method of coating such glass plates with a thin film of plasma polymer was developed such that portion 3 of the scattering curve is greatly reduced for the resultant cured epoxy films.

In order to obtain information concerning the spatial elucidation of crosslinks, epoxy networks were synthesized with varying proportions of Sn containing diamine (providing a heavy atom labeled crosslink) and a monoamine chain extender. No peak, ascribable to heavy atom-heavy atom interactions was found in the SAXS or wide angle x-ray scattering pattern, apparently because of the very broad distribution of crosslink to crosslink distances.

FOREWORD

The project was carried out under the direction of Dr. A. Schindler, principal investigator and Dr. N. Morosoff, co-principal investigator. Dr. Schindler was responsible for overall coordination of the program and synthesis of cured epoxy resins, Dr. Morosoff for obtaining and interpreting the x-ray scattering data. Other participants were Gregory Whitaker who carried out the x-ray scattering measurements and routine x-ray scattering analysis and prepared epoxy resins, Joyce Pusel who aided in the synthesis of heavy atom intermediates, and John Guill who deposited the plasma polymer film which was used as a release interface in the preparation of some of the epoxy films.

The authors are also indebted to Dr. R. Seltzer, Ciba-Geigy, Ardsley, New York, for supplying the epoxides used in this study.

Dr. W. R. Krigbaum, Department of Chemistry, Duke University, Durham, North Carolina, acted as consultant on x-ray investigations. The authors wish to express their appreciation for his assistance during the course of investigations.

The Project Engineer was Mr. Freeman F. Bentley of the Air Force Materials Laboratory and his helpful discussions are gratefully acknowledged.

The interim report was published as AFML-TR-78-186.

TABLE OF CONTENTS

	<u>Page</u>
2.0 Introduction	1
2.1 Objective	1
2.2 Scope of Work	1
3.0 Problem Definition and Approach	2
3.1 Network Inhomogeneities	2
3.1.1 Background	2
3.1.2 Small Angle X-Ray Scattering	6
3.2 Crosslink Density Distribution	9
4.0 Preparation of Cured Resin Samples	21
4.1 Curing Procedure	21
4.2 Resin Formulations	22
4.3 Labeled Resin Components	27
5.0 X-Ray Scattering	33
5.1 Interpretation of X-Ray Scattering Data	33
5.1.1 Desmearing of Slit Collimated X-Ray Scattering Data	33
5.1.1.1 Correction for Width Smearing	35
5.1.1.2 Correction for Length Smearing	36
5.1.1.3 Desmearing for an Infinite Beam	39
5.1.1.4 Desmearing for a Finite Beam	39
5.1.1.5 Slit Length Desmearing at RTI Using the Spline Function Approximation of the Scattering Curve for Numerical Differentiation	41
5.1.1.6 Spline Function Approximation of Scattering Curve for Numerical Differentiation	41

TABLE OF CONTENTS (Continued)

	<u>Page</u>
5.1.2 Information Attainable from SAXS	44
5.1.3 Angular Nomenclature	45
5.1.4 Guinier Plot	45
5.1.4.1 Effect of Polydispersity	49
5.1.4.2 Effect of Interparticle Interference	49
5.1.5 The Invariant and Scattering Power of the Sample	50
5.1.6 Determination of the Invariant, the Specific Surface, and Uniformity of Electron Density Over Small Distance .	51
5.1.7 The Correlation Function, Specific Volume, and Transversal Lengths and Correlation Distance	52
5.1.8 Swelling Sample as a Means of Modifying SAXS	59
5.1.9 Application of Heavy Atom Tagging to Spatial Distribu- tion of Crosslinks	59
5.2 Results of X-Ray Scattering Measurements from Cured Epoxy Samples	61
5.2.1 Introduction	61
5.2.2 Experimental Results	64
5.2.2.1 Protocol for Collection of SAXS Data for Cured Epoxy Samples	64
5.2.2.2 Results Obtained for Samples Cast on Frekote Coated Plates	69
5.2.2.3 Results Obtained for Samples Cast on Fluorinated Glow Discharge Polymer Coated Plates	75
5.2.2.4 X-Ray Scattering From Samples With Varying Crosslink Density	76

TABLE OF CONTENTS (Continued)

	<u>Page</u>
5.3 Conclusions	77
References	80

LIST OF ILLUSTRATIONS

<u>Figure</u>	<u>Page</u>
1. Schematic representation of an ideal network derived from tetrafunctional and difunctional components in stoichiometric ratio	15
2. Schematic representation of a network from tetrafunctional and difunctional components with some of the tetrafunctional components exercising a functionality of two	17
3. Schematic representation of a network derived from tetrafunctional and difunctional components with two of the tetrafunctional molecules exercising a functionality of three . . .	18
4. Incident beam profile plotted versus m	34
5. a) Schematic representation of the x-ray scattering experiment	38
b) Intersection of the scattered x-rays with the registration plane for a slit collimated beam	38
6. Typical Kratky camera incident beam profile at registration plane	40
7. The atomic scattering factor of copper	47
8. A representation of the function $\bar{V}(r)$	54
9. The function $\lambda_0(r)$ for a sphere of radius R	55
10. Physical concept of the transversal length	56
11. Plot of $\log I(m)$ versus $\log m$	63
12. Plot of scattering power versus $\tilde{I} \cdot m^3/x$	74

LIST OF TABLES

<u>Table</u>	<u>Page</u>
1. Epoxy Resins Prepared from a Triepoxide (Ciba-Geigy PT-810) by Anhydride Cure in the Presence of Unreactive Diluents	24
2. Epoxy Resins Prepared from a Triepoxide (Ciba-Geigy PT-810) by Anhydride Cures at Different Temperatures	26
3. Epoxy Samples Prepared from Diepoxides by Anhydride Cures at Different Temperatures	28
4. Formulations for Araldite 6004 Cured with Dibutyltin Bis(3-aminopropyl)/hexylamine	31
5. Duration of Data Collection for Sample T-1	66
6. Preparation of Cured Epoxy Samples for SAXS	71
7. Analysis of SAXS Data for Cured Epoxy Samples Prepared as Described in Table VI.	72
8. Bragg Spacings for Peaks in WAXS Photographs	78

1.0 Summary

Small angle x-ray scattering (SAXS) and wide angle x-ray scattering (WAXS) techniques were applied to investigate and characterize cured epoxy resin inhomogeneities on the one hand and to elucidate the spatial distribution of crosslinks on the other. Priority was given to the first problems, i.e., network inhomogeneities.

Methods were developed to obtain and interpret the x-ray scattering at very low scattering angles where the scattered intensity increases markedly with decreasing scattering angle. The low scattering power of this feature is consistent with the small difference in density between cured and uncured epoxy resins.

Such scattering was analyzed for several sets of epoxy-hardener systems, each cured at three curing temperatures. For one such system using two curing temperatures, each cure was also reproduced with a change in release interface followed by SAXS analysis of the resultant film. The results demonstrated that the analyzed scattering feature was associated with the surface rather than with the bulk of the sample.

Epoxy resins were cured with varying proportions of heavy atom containing diamine (to provide a heavy atom labeled crosslink) and monoamine chain extender. No peaks in the x-ray scattering pattern of such systems ascribable to heavy atom-heavy atom interactions were found.

2.0 Introduction

2.1 Objective

The principle objective of this program is the development of methods based on x-ray scattering techniques which permit to address crosslink density distributions in cured epoxy resins.

2.2 Scope of Work

The objective of the program involves two separate problems which require different approaches. The first problem concerns the dimensional characterization of network inhomogeneities and the correlation of the degree of inhomogeneity with resin formulation and curing conditions. The second problem concerns the elucidation of the spatial distribution of crosslinks. Further work would then permit to correlate the established crosslink density distributions with physical properties of the cured resin. Both problems are being addressed by utilizing wide angle (WAXS) and small angle (SAXS) x-ray scattering techniques.

Priority was given to the first problem, the investigation and characterization of network inhomogeneities. This selection was made because of the general importance of this problem as manifested by a number of recent publications dealing with nodule formation in cured epoxy resins.

3.0 Problem Definition and Approach

3.1 Network Inhomogeneities

3.1.1 Background

Considerable evidence has been accumulated by different investigators which demonstrates that the crosslink density in highly crosslinked polymeric networks is not uniform. The nonuniformity of the network density can be so pronounced that the system approaches a two-phase system being composed of a large number of densely crosslinked domains of globular shape (nodules or network clusters) which are imbedded in a common matrix of lower crosslink density. Indeed, Funke (1) states in a discussion of reaction mechanisms leading to the formation of crosslinked systems that the formation of homogeneous networks represents an exception in crosslinking polymerization.

Funke (1,2) summarizes several factors which can be responsible for the formation of network inhomogeneities in crosslinking polymerizations.

1. Difference between the reactivities of different functional groups which results in a uneven distribution of crosslinks.
2. Phase separation (microsyneresis) due to thermodynamic instability of the system.
3. Phase separation due to steric hindrance
4. Intramolecular cyclization reactions
5. Unreacted functional groups.

The importance of individual factors depends on the system under consideration, but generally, all of the factors can play a decisive role in the curing process of epoxy resins.

Uneven distribution of crosslinks caused by differences between the reactivities of different functional groups will be affected by the

chemical structures of the components of the resin formulation (e.g., monoepoxides vs. diepoxides, primary vs. secondary amines, ether vs. ester formations in anhydride cures, etc.).

Microsyneresis is a consequence of partial segregation occurring in a system on approaching its limit of thermodynamic stability. It will be mainly of importance in systems containing unreactive diluents. As shown by Dusek (3,4) a network formed in the presence of a solvent can accommodate only an amount of the latter corresponding to its swelling equilibrium value. With increasing crosslinking density the degree of swelling of the network decreases and phase separation will occur which may be enhanced by incompatibility between solvent and polymer. Microsyneresis will be affected by reaction temperature and ultimate crosslink density, as well as solubility parameters of solvent and polymer.

The occurrence of microsyneresis is not restricted to systems containing an unreactive diluent but can take place in any system in which limited compatibility between network and monomeric resin exists. Indeed, a limited compatibility between network and uncrosslinked resin is assumed by several authors to explain the formation of network inhomogeneities.

Phase separation due to steric hindrance can be caused by two effects (5). Firstly, already at moderate degrees of crosslinking, residual functional groups can become separated too far to undergo further reaction. Secondly, with increasing degree of crosslinking the glass transition temperature of the polymer increases due to increasing immobilization of network segments. Consequently, as soon as the glass transition temperature approaches the curing temperature further curing reactions cease. By increasing the curing temperature renewed segmental mobility is obtained and further curing takes place (6).

A relatively low importance was assigned by Dusek et al. (7) to cyclization reactions in epoxy cures which should result in the formation of microgels. The authors claim this type of reaction to be more typical of crosslinking chain polymerizations where, at higher contents of crosslinking agent, densely crosslinked particles are already formed at the beginning of the reaction.

Contrarily to Dusek et al. (7), Lüttgert and Bonard (8) claim that the decisive factor determining the morphology of cured epoxy resins is given by the number of microgel particles formed during the very early stages of the curing process. According to these authors the onset of crosslinking occurs localized with the formation of microgel particles of high crosslink density. As the curing process proceeds, these gel particles grow in size in the liquid resin until they meet and the bulk of the material gels. Consequently, the final size of globular domains in the cured resin depends on the ratio of two rates, the rate of microgel formation (nucleation) and the rate of growth of the gel particles. At high curing temperatures the rate of nucleation will be fast and the great number of microgels formed permits growth only to a small size. Low curing temperatures initiate only a small number of gel particles and the cured resin will show large globular inhomogeneities. The proposed curing mechanism is based on results obtained from electron microscopic investigations of fracture surfaces of resins cured at different temperatures.

The existence of inhomogeneities in highly crosslinked polymer networks, especially cured epoxy resins, is supported by a wide range of experimental evidence. Swelling experiments (9, 10) indicated differences between the rates of solvent uptake for globules and matrix mater-

ial. Mechanical properties, such as tensile strength, showed large discrepancies between theoretical and experimental values which were interpreted by assuming network inhomogeneities (11).

Most of the evidence is derived from electron microscopic investigations of fracture surfaces by replication technique (7,8,12-19). Generally, the micrographs reveal the presence of globular domains with dimensions in the range of 10-70 nm. Since the presence of nodules was also observed with other polymeric networks besides epoxy resins (20-23), nodule formation can be considered as characteristic for crosslinking polymerization reactions. Micrographs of fracture surfaces of uncross-linked, glassy polymers, such as polystyrene or poly(methyl methacrylate), reveal similar features but in a less pronounced way (24).

So far the existence of nodular structures in cured epoxy resins could not be confirmed by x-ray scattering experiments (7,16,17). In view of the accumulated evidence for the presence of globular network inhomogeneities the lack of x-ray evidence would indicate a very small difference between the electron densities of nodules and embedding matrix material. This conclusion is not inconsistent with the suggestion that the microscopically observed nodules represent regions of higher crosslink density, for an increase in the latter may only slightly affect the local electron density (17).

An essentially uniform electron density throughout the bulk of cured epoxy resins is also indicated by the absence of structural features in transmission electron microscopy of microtomed samples (25). Apparent regions of high crosslink density at the edge of a craze were observed by transmission electron microscopy of an amine cured epoxy resin (26), but the large dimensions of these regions (200-1000 nm) are

far outside the range of nodule dimensions generally observed on fracture surfaces.

3.1.2 Small Angle X-Ray Scattering

A detailed discussion of SAXS as applied in the morphological investigations of cured epoxy resins will be given in a later section. In this section only some principles are discussed which affect sample selections and preparations.

For the purpose of our investigations a cured epoxy resin possessing an inhomogeneous network structure (nodules) may be considered to correspond in its x-ray scattering effects to a system composed of low molecular weight solvent in which particles of colloidal dimensions are dispersed. The colloidal particles of the model system would correspond to the densely crosslinked nodules whereas the solvent corresponds to the matrix of uniform low crosslink density. In such a system the total SAXS effect is composed of three contributions (27).

(a) The scattering of the solvent (matrix) which is generally very weak in the small angle region. (b) The actual particle scattering which can be observed only if a sufficient difference in electron densities exists between particles (nodules) and solvent (matrix). The intensity of the scattered radiation generally increases with decreasing scattering angle. From the shape of the intensity distribution close to the primary beam conclusions can be derived with respect to shape and size of the scattering particles. (c) Density fluctuation inside the particles cause a constant background intensity in the small angle region.

The intensity of the particle scattering depends on the magnitude of the electron density difference between both phases. This difference

is rather small in cured epoxy resins. Dusek et al. (7) estimated a value not exceeding 0.005 mol/cm^3 , i.e., the difference between the densities of nodules and matrix would be smaller than 0.01 g/cm^3 . Because of this small density difference the intensity of sample scattering deviates only slightly from the background intensity resulting from instrumental scattering.

Initially, it was intended to investigate epoxy resins cured with hardeners containing heavy atoms of high x-ray scattering power (e.g., chlorine, bromine, tin). This approach was abandoned since an increase in the electron density difference between nodules and matrix cannot be achieved by this method. It seems reasonable to assume that the difference in crosslink densities between nodules and matrix will not be affected to a large extent by the kind of hardener used. Since the difference in crosslink densities determines the difference in electron densities an increase in contrast between nodules and matrix will not be achieved with the use of labeled hardeners.

Labeled hardeners of high x-ray scattering power would be useful in the present study only if they were selectively distributed between the two phases of the cured resins. Such a possibility might be realized by using a combination of labeled and unlabeled hardeners of strongly differing reactivities in the curing process. If one assumes the nucleation theory of Lüttgert and Bonart (8) to apply, the more reactive hardener should preferentially participate in the initial formation of the microgel particles. Such a system would be given by dichloromaleic anhydride and maleic anhydride where the former compound cures considerably faster than the latter. As a consequence the core of the nodules should have a higher chlorine concentration than the matrix and the particle scattering power of the resin should be increased.

Although the outlined resin preparation might result in improved particle scattering, the interpretation of SAXS data of such samples cannot be generalized due to the complexity of the curing system. The electron density difference between nodules and matrix can be increased in resins cured with conventional hardeners by utilizing the effect of crosslink density on the swelling properties of crosslinked networks. The solvent uptake by the less densely crosslinked matrix will be higher than by the more densely crosslinked nodules. Consequently, the use of a swelling agent of high electron density, such as brominated aliphatic or aromatic hydrocarbons, will generate the desired electron density difference and increase the particle scattering of the sample.

Since the required contrast between nodules and matrix cannot be achieved with labeled hardeners unlabeled hardeners were used in most of our resin preparations. The use of conventional hardeners has the advantage that resin formulations and curing conditions can be investigated which are close or even identical to those applied in practical applications.

Labeled hardeners, especially brominated anhydrides, also present experimental problems in sample preparations. The high molecular weights of the hardeners require resin formulations which often exceed the solubility limit of the hardener in the epoxy resin. This unfavorable situation is aggravated by the high melting points of brominated anhydrides which require elevated casting temperatures with the possibility of premature gelling of the resin.

The extremely small electron density difference between nodules and matrix of conventionally cured epoxy resins required the development of a sophisticated experimental technique for our SAXS investigations. For

this purpose conditions of sample preparation were selected which could be anticipated to yield networks possessing different degrees of inhomogeneity.

3.2 Crosslink Density Distribution

The elucidation of the crosslink density distribution in cured epoxy resins has already been addressed in part by the evaluation of the observed intensity distribution caused by particle scattering in SAXS experiments. These experiments reveal the presence of domains with crosslink density exceeding that of the surrounding material and thus demonstrate for such resins a bimodal form of the overall crosslink density distribution.

Experimental determinations of distances between crosslinks in polymeric networks were performed recently with model networks utilizing SAXS (28,29) and neutron coherent scattering (29,30) techniques. The model networks for SAXS were prepared by anionic polymerizations which yielded monodisperse chain segments of predetermined lengths which could be connected by ironlabeled crosslinks during network formation. SAXS by these networks revealed the presence of one single but rather broad diffraction band. For a given network the position of the band maximum was found to be a function of the degree of swelling of the gel. For a series of networks differing merely in the average segment length between crosslinks the maximum shifted to lower scattering angles as the average segment length increased.

It followed from these SAXS results that a well-defined correlation distance exists between first neighbor crosslinks. There is, however, no correlation between the position of second neighbor crosslinks: the network behaves in this respect as amorphous compounds or as liquids (29).

The application to cured epoxy resins of the outlined SAXS technique for structural investigations of model networks requires some further considerations. The most pronounced difference between both kinds of networks is given by the extremely high crosslink density in epoxy resins.

In the model networks the observed Bragg spacings corresponding to the average distances between crosslinks varied between 10 and 20 nm. These values are about one order of magnitude larger than can be estimated for crosslink distances in cured epoxy resins which have to correspond to the molecular dimension of one epoxy-hardener pair. As a consequence, the positions of the intensity maximum in the diffractogram representing the average Bragg distance of crosslinks will occur in the wide angle region and will coincide with intensity maxima caused by general short range intra- and intermolecular ordering in the network. The latter maxima were found by Dusek et al. (7) to correspond to Bragg distances of about 0.5 and 1.5 nm in a resin derived from the diglycidyl ether of bisphenol-A.

In principle, the strong overlap or near coincidence of both, the amorphous scattering of the resin and the scattering due to the labeled crosslinks, can be resolved by subtracting the scattering curves of two resins prepared under identical conditions but possessing labeled and unlabeled crosslinks, respectively. The method will be subjected to some inaccuracy since short range ordering in both samples will differ to some extent due to the presence and absence of the labeling atoms.

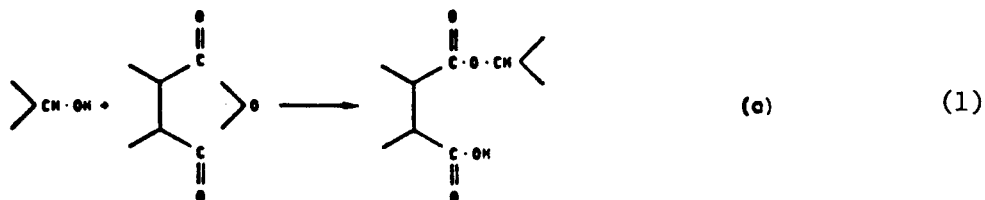
Furthermore, the evaluation of the scattering curves will be affected by any difference between both samples concerning the extent of network inhomogeneities. For this reason the elucidation of particle scattering

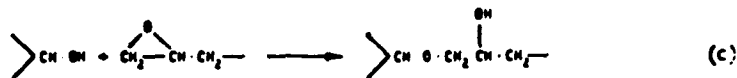
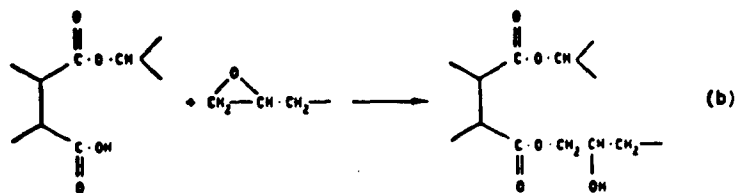
was assigned priority in our work in order to characterize film samples prior to further detailed investigations.

According to the synthetic method used for the preparation of model networks,^{28,29} the functionalities of the iron labeled centers varied to some extent but it could be assumed that each center will have a functionality exceeding a value of two, i.e., each labeled center will represent a crosslink in the network. This necessary condition for the elucidation of crosslink densities by x-ray scattering techniques is not met by epoxy resins containing labeled crosslinks.

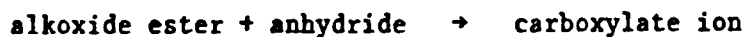
In order to simplify the discussion, only network formations will be considered which occur between difunctional and tetrafunctional components. Such network formations are represented by cures of diepoxides with either anhydrides of dicarboxylic acids or primary diamines.

Anhydride cures in the absence of catalyst require the presence of hydroxyl groups in the epoxy resin, e.g., secondary hydroxyls found in the higher molecular weight epoxides based on bisphenol-A. According to Fisch *et al.* (6,31) the anhydride ring is opened by the hydroxyl group under formation of a half-ester, eq. (1a). The half-ester then reacts through its acid group with a second epoxy ring thereby forming a hydroxy diester, eq. (1b). The hydroxyl group of the diester can be consumed either in further esterification reactions with anhydride groups or can undergo etherifications reactions with epoxide groups, eq. (1c).

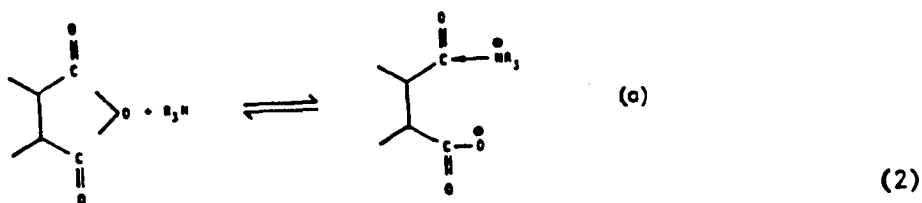




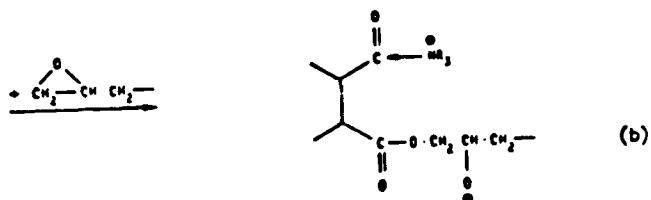
Undesirable etherification reactions can be suppressed by tertiary amine catalysis of the curing process. Tanaka and Kakiuchi (32) concluded from their kinetic analysis of base-catalyzed curing processes that etherification did not occur below 140°C. The reaction sequence for tertiary amine catalyzed cures as suggested by Fischer (33) involves the alternating formation of alkoxide esters and carboxylate ions.

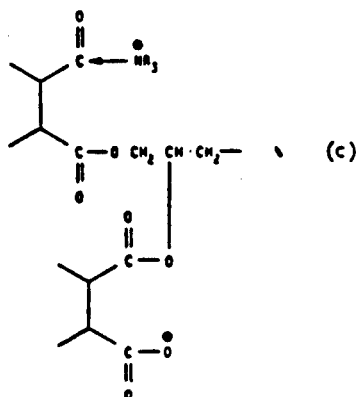
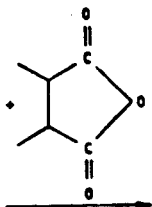


as shown in eq. (2).



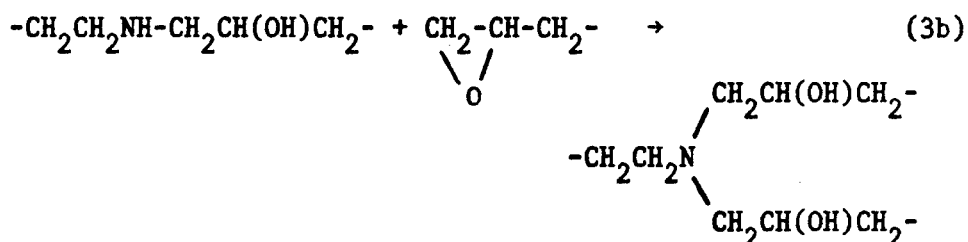
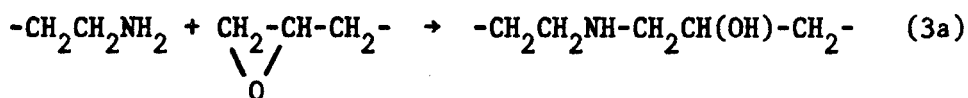
(2)





Provided one uses well defined epoxy resins free of hydroxyl groups and pure anhydrides free of carboxyl groups, curing will not occur even at elevated temperatures prior to the addition of the amine catalyst. This is of special importance for the formulation of high melting epoxides and anhydrides.

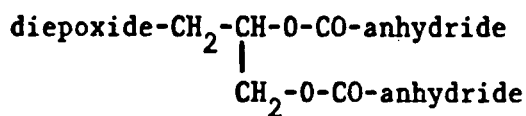
In amine cures the functionalities of hardener and resin are reversed with respect to anhydride cures, the primary diamine being tetrafunctional and the diepoxide being difunctional. At stoichiometrically equivalent ratios of functional groups or in the presence of excess amine, the consecutive reaction of the epoxide groups with the hydrogen atoms of the amino groups is the only reaction taking place (34).



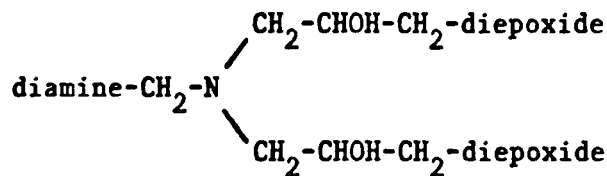
If epoxide groups are present in excess, the hydroxyl groups formed in the reaction can participate in the formation of ether linkages (34).

With both curing mechanisms, anhydride and amine cure, networks of maximum crosslink density should result under ideal conditions if tetra and difunctional components are used in stoichiometric ratio and if the tetrafunctional component fully exercises its functionality. From a structural point of view these networks are identical for both curing mechanisms. A two-dimensional representation of such an ideal network is shown in Figure 1 where tetra and difunctional components are designated by rectangles and circles, respectively.

The actual crosslinks as defined by the branching points of the chains have different chemical structures depending on the curing mechanisms. In anhydride cures one obtains



whereas primary diamine cures yield



It is obvious that the branch point cannot be labeled for x-ray work but only some part of the molecule of the tetrafunctional component. This means the network is labeled by the rectangles in the schematic presentation of Figure 1.

Actual network structures of cured epoxy resins will deviate considerably from the idealized structure of Figure 1. These deviations will be a consequence of not all of the functionalities of both components being fully exercised. Because of its high irregularity such a network is difficult to depict in a two-dimensional representation, especially concerning the spatial distributions of the tetrafunctional component.

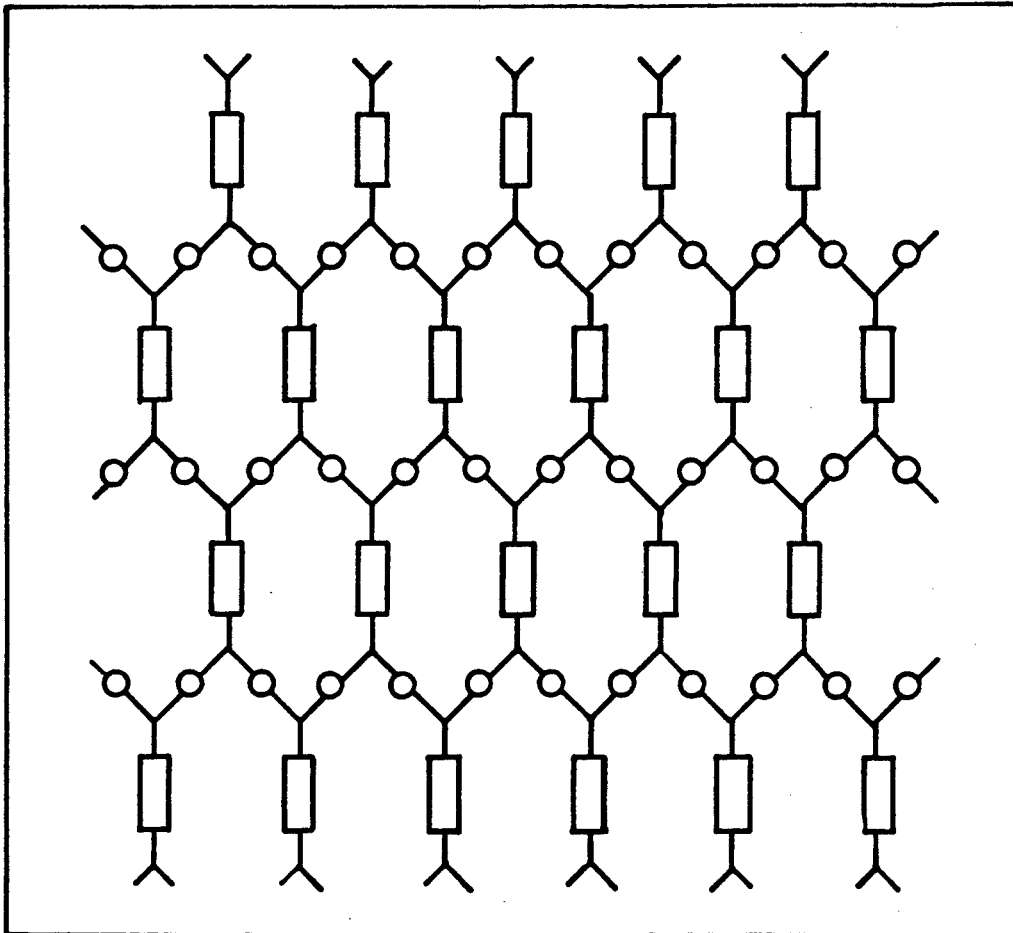


Figure 1. Schematic representation of an ideal network derived from tetrafunctional (rectangles) and difunctional (circles) components in stoichiometric ratio.

In Figure 2 two network irregularities are schematically indicated where one tetrafunctional moiety, depicted as a solid rectangle, acts only difunctional. In the schematic network of Figure 3, two tetrafunctional molecules act only trifunctional. In both cases the mesh size of the network is increased by the incomplete reaction of the tetrafunctional component, i.e., the crosslink density is decreased. Incomplete reactions of the tetrafunctional components with concomitant changes in crosslink densities will have only a minor effect on the x-ray scattering properties of samples prepared with labeled tetrafunctional compounds. Each labeled molecule would contribute to the scattered intensity irrespective of its functionality in the network, i.e., participation of a labeled component in either crosslinking or chain extension could not be distinguished.

The effect of differences in crosslink densities on x-ray scattering properties of labeled samples will be enhanced by swelling in solvents of low electron density. The lower the crosslink density the more the network will expand thereby increasing the average distance between chains. In highly swollen regions the intermolecular correlation between scattering centers may be lost and only the intramolecular correlation will remain representing the alternation of labeled and unlabeled moieties in the chains. In densely crosslinked (less swollen) regions intramolecular correlation between scattering centers might persist and permit the estimation of crosslink density distributions in these regions.

The basic problem in the elucidation of crosslink densities in cured epoxy resins is given by the fact that changes in crosslink density are solely caused by the polyfunctional compound not exercising its maximum functionality. Since irrespective of the degree of functionality exercised, polyfunctional and difunctional components alternate in the

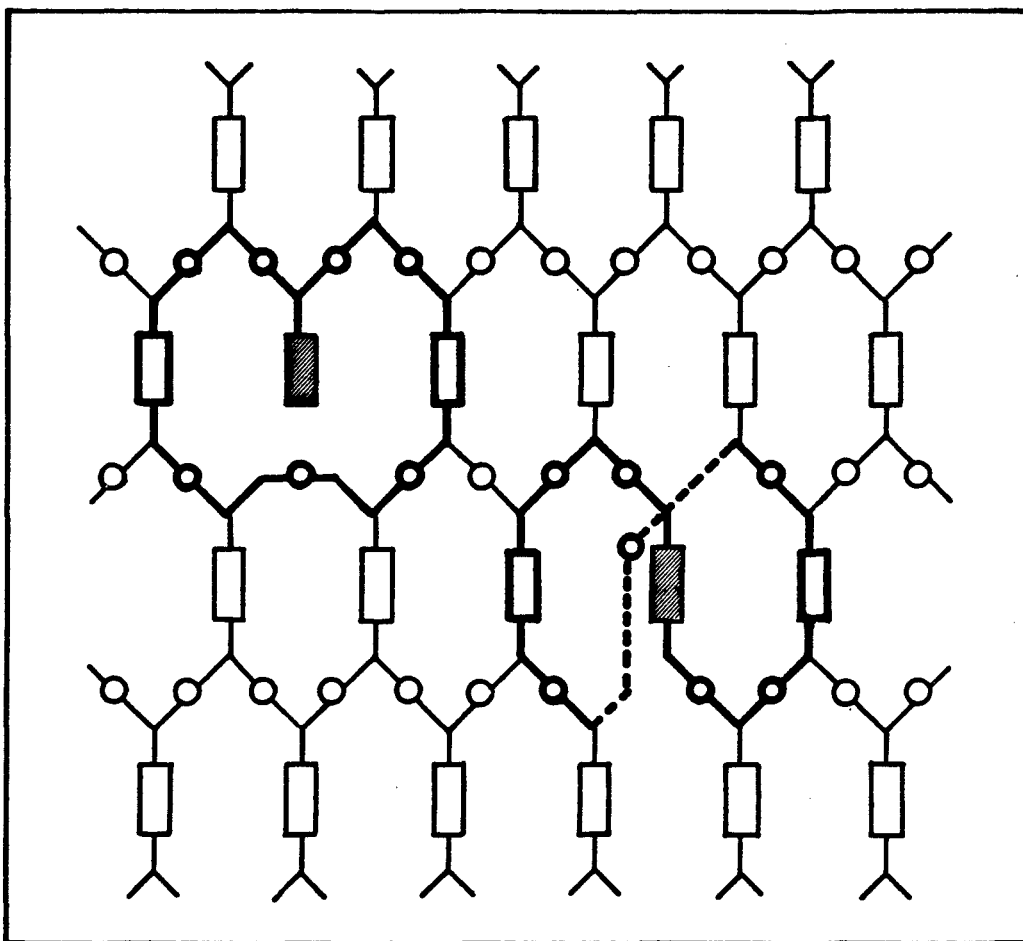


Figure 2. Schematic representation of a network derived from tetrafunctional (rectangles) and difunctional (circles) components with some of the tetrafunctional components exercising a functionality of two.

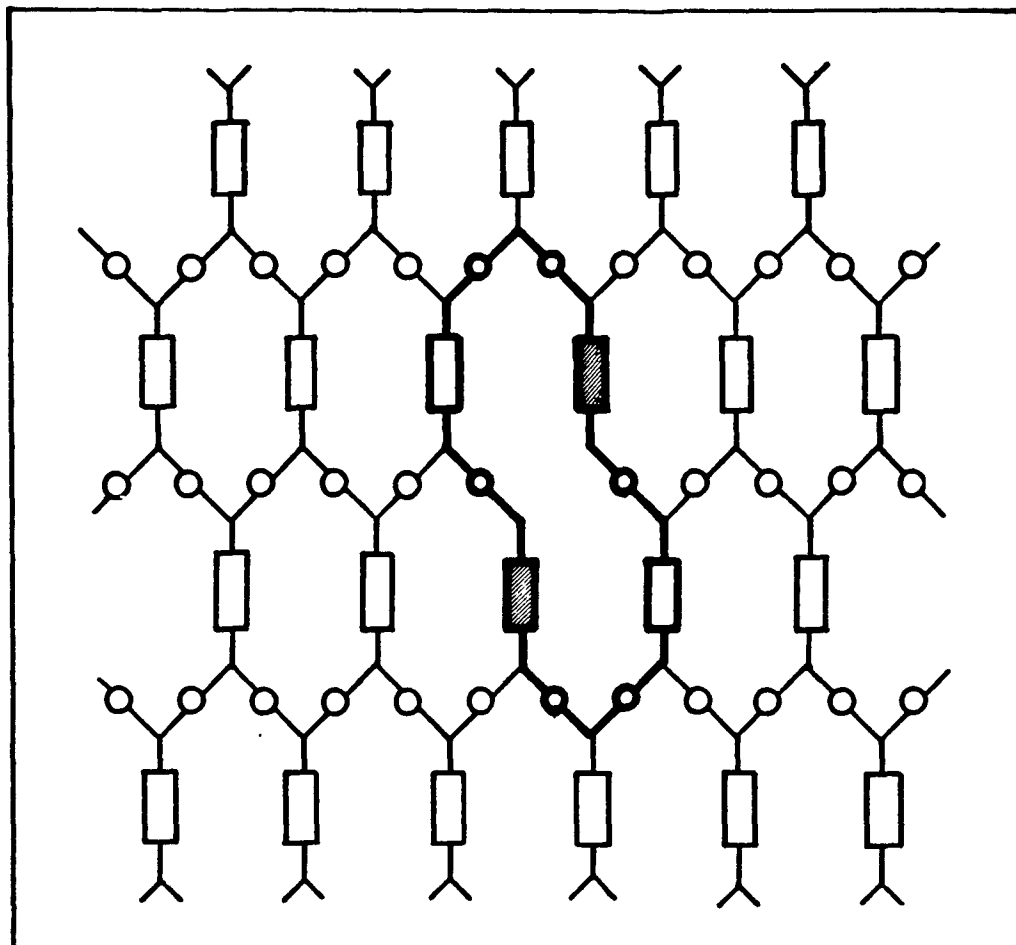


Figure 3. Schematic representation of a network derived from tetrafunctional (rectangles) and difunctional (circles) components with two of the tetrafunctional molecules exercising a functionality of three.

network chains crosslinks cannot be distinguished from chain extension by labeling the polyfunctional component with centers of high x-ray scattering power. Indeed, for the suggested x-ray investigations on swollen films it is irrelevant whether the polyfunctional or the difunctional component has been labeled with heavy atoms.

The interpretation of x-ray scattering results would be greatly simplified with systems in which the scattering centers are exclusively inserted at the crosslinks. Appropriate systems approaching this condition would be given by resin formulations containing reactive diluent (chain extenders) such as mono and diepoxide for anhydride cures with the diepoxide being labeled. Correspondingly, in amine cures of diepoxides one would have to use secondary diamine in combination with labeled primary diamine (11).

The curing mechanism of such systems strongly resembles the crosslinking mechanism in free radical polymerization of mono and divinyl compounds. In the latter mechanism crosslink density and crosslink density distribution are determined by the copolymerization behavior of both components, i.e., by the values of their respective copolymerization parameters. This applies also for the curing mechanism of epoxy systems. In anhydride cures the reactivities of mono and diepoxide toward the anhydride will be different and copolymerization parameters can be assigned to both components thus permitting to describe the system by the usual copolymerization equation. The more reactive component will be consumed faster and the crosslink density will change to some extent as the curing process proceeds. Analogous considerations apply to amine cures with the secondary diamine corresponding to the monoepoxide in anhydride cures and the primary diamine corresponding to the diepoxide.

By varying the proportions of difunctional diluent in the resin formulations, networks can be prepared differing in their crosslink

densities. The range of crosslink densities can be extended from weakly crosslinked systems for which rubber elasticity theory still applies to densely crosslinked systems for which the theory fails. On these systems crosslink density distributions should be accessible by x-ray scattering techniques provided the distribution of crosslink distances is not too broad.

4.0 Preparation of Cured Resin Samples

4.1 Curing Procedure

X-ray scattering experiments require only small samples of 1 x 4 cm in size. The thickness of the samples should be uniform and should not exceed an optimum value depending on the chemical composition of the resin which determines its x-ray absorbance. The latter condition is only of importance for samples containing heavy atoms, samples prepared with conventional resins formulations were generally made of thickness below the optimum value to allow for uptake of brominated solvents in swelling studies. Differences in sample thicknesses are not critical since our SAXS intensities are normalized for the same primary beam intensity.

The formulated resins are cured between glass plates using thin Silastic or Teflon tubings as gaskets. During the initial part of our studies severe problems were encountered with the release of the cured samples from the plates. This problem has been solved by proper plate treatment.

Clean glass plates are evenly sprayed with Frekote 34 (Frekote, Inc., Boca Rota, Fla.) and air-dried. The plates are then baked for 5-6 hrs at 230-250°C in a glass annealing oven. After cooling to ambient temperature the plates are ready for one-time use. For reuse the plates have to be cleaned and recoated since some of the Frekote coating is transferred to the resin surface as indicated by its hazy appearance.

Epoxy resin and anhydride are weighed in a glove bag under nitrogen to prevent access of humidity. Screw cap vials of 20 ml capacity are used. Depending on the melting points of epoxide and anhydride, the closed vials are sufficiently heated with an air gun to obtain a homo-

genous blend which is then degassed in a vacuum oven set at proper temperature to keep the resin viscosity sufficiently low. After degassing tertiary amine accelerator (dimethyl benzylamine) is added via a microsyringe and carefully blended without reintroducing air bubbles.

The blended resin is cast on a prepared glass plate at the center of a Silastic ring. The mold is closed with a second plate and is secured with binder clips. Formulations with high melting epoxides or anhydrides require preheated plates to prevent recrystallization of the compounds.

Curing is performed by placing the plates upright in a thermostated circulating air oven. After the required curing period the molds are slowly cooled to ambient temperature and pried open.

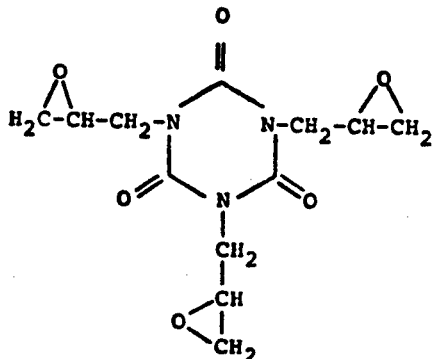
An alternative method providing excellent mold release was found to be plasma deposition of extremely thin (0.01 - 0.1 μm) polymer layers on glass surfaces. Among the deposited polymers tested, those derived from either tetrafluoroethylene or perfluorodibutyltetrahydrofuran showed outstanding release properties. Especially the latter polymer permitted repeated use of the glass plates without recoating and the cured epoxy films possessed mirror finish.

4.2 Resin Formulations

In order to test the applicability of SAXS techniques for the elucidation of network morphologies, resin formulations and curing conditions were selected for which large variations in the extent of network inhomogeneities could be anticipated. A triepoxide, PT-810 (Ciba-Geigy) was considered most appropriate for this purpose and a

considerable number of samples was prepared under varying conditions listed in Tables 1 and 2.

The triepoxide of structural formula



is a relatively well defined compound with a narrow melting range around 125°C. The reported molecular weight per epoxy group is in the range of 102-109 in fair agreement with the theoretical value of 99.

In Table 1 are summarized resin preparations in which varying amounts of unreactive diluents were used. These experiments were designed to observe possible effects of microsineresis on nodule formation in the resins. The diluents were selected for high boiling points and for solubility parameters in the range of 10-11 $\text{cal}^{1/2}/\text{cm}^{3/2}$ (0.0205-0.0226 $\text{J}^{1/2}/\text{m}^{3/2}$) to assure initial compatibility with the resin. The diluents were

<u>Diluent</u>	<u>Boiling Point</u> (°C)	<u>Solubility Parameter</u> ($\text{cal}^{1/2}/\text{cm}^{3/2}$)
Dibutylphthalate (DBP)	340	9.9
Dimethylphthalate (DMP)	283	11.0
Tetrabromoethane (TBE)	240	10.3

With bis(2-methoxyethyl)ether (bp=162°C) it was not possible to obtain bubble-free samples in 140°C cures. Tetrabromoethane was used as

Table 1. Epoxy resins prepared from a triepoxide (Ciba-Geigy PT-810) by anhydride cure in the presence of unreactive diluents.

Sample Designation	Anhydride		Diluent		Hours Cured At		
	Kind	R _H	Kind	ml/g	80°C	120°C	140°C
D-1	THPA	0.9	DMP	0.88	-	15	-
D-2	THPA	0.9	DMP	0.44	-	15	-
D-3	THPA	0.9	DMP	0.22	-	15	-
K-1	DCMA	0.9	DMP	1.00	-	19	-
K-2	DCMA	0.9	DMP	1.00	3	14	-
K-3	DCMA	0.6	DMP	0.88	-	16	-
K-4	DCMA	0.6	DMP	0.88	2	14	-
K-5	DCMA	0.9	DMP	1.00	2	14	-
L-1	DBTHPA	0.9	DMP	0.54	93	6	-
L-2	DBTHPA	0.6	DMP	0.54	93	6	-
M-1	DBTHPA	0.9	DBP	0.54	16	-	-
M-2	DBTHPA	0.9	DBP	0.54	16	-	-
N-1	DBTHPA	0.9	DMP	0.54	25	-	-
N-2	DBTHPA	0.9	DMP	0.54	17	4	4
N-3	DBTHPA	0.9	DMP	0.54	17	8	-
R-1	NMA	0.6	TBE	0.03	24	-	-
R-2	NMA	0.6	TBE	0.07	24	-	-
R-3	NMA	0.6	TBE	0.03	16	8	-
R-4	NMA	0.6	TBE	0.07	16	8	-
R-5	NMA	0.6	TBE	0.03	16	4	4
R-6	NMA	0.6	TBE	0.07	16	4	4

Anhydrides: THPA = Tetrahydrophthalic anhydride
 DCMA = Dichloromaleic anhydride
 DBTHPA = Dibromotetrahydrophthalic anhydride
 NMA = Nadic methyl anhydride

R_H = mol anhydride/mol epoxy group

Diluents: DMP = Dimethyl phthalate
 DBP = Dibutyl phthalate
 TBE = Tetrabromo ethane

a labeled diluent in order to observe the possible formation of solvent clusters in the cured resin.

In Table 2 are summarized curing conditions for resins prepared from PT-810 triepoxide in the absence of diluents. In these preparations different curing temperatures were used to affect network morphology. This approach would be in accordance with the nucleation theory of Lüttgert and Bonart⁸ discussed previously.

All sample preparations based on PT-810 were made by anhydride cures including unlabeled (tetrahydrophthalic anhydride and methyl nadic anhydride) and labeled anhydrides (dichloromaleic anhydride and dibromotetrahydrophthalic anhydride). Two molar ratios of anhydride to epoxy groups, $R_H = 0.9$ and 0.6 , were applied. At the higher ratio the amount of anhydride nearly suffices for the triepoxide to fully exercise its maximum functionality of six. At the lower ratio the average functionality of the triepoxide will be four. Also in this case highly cross-linked networks result but with enhanced probability for the formation of inhomogeneities since during the early stage of the curing process part of the tri-epoxide will exert its maximum functionality due to the initial abundance of anhydride.

Since one might argue that the selected resin formulations are favorable for nodule formation, several samples were prepared from diepoxides by anhydride cure utilizing a slightly increased mol ratio of anhydride/epoxy groups of 0.95 . The epoxy resins used were a diglycidyl ether of bisphenol-A (Araldite 6004, Ciba-Geigy), and two cycloaliphatic diepoxides, 3,4-epoxy-6-methylcyclohexylmethyl adipate (CY-178, Ciba-Geigy)

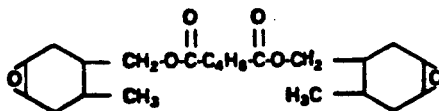


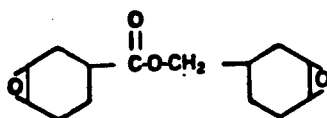
Table 2. Epoxy resins prepared from a triepoxide (Ciba-Geigy PT-810) by anhydride cures at different temperatures.

Sample Designation	Anhydride		Hours Cured At				
	Kind	R_H	80°C	120°C	130°C	140°C	180°C
D-4	THPA	0.9	-	4	-	-	-
P-1	NMA	0.9	25	-	-	-	-
P-2	NMA	0.9	17	8	-	-	-
P-3	NMA	0.9	17	4	-	4	-
P-4	NMA	0.6	25	-	-	-	-
Q-1	NMA	0.9	26	-	-	-	-
Q-2	NMA	0.9	18	8	-	-	-
Q-3	NMA	0.9	18	4	-	4	-
Q-4	NMA	0.6	26	-	-	-	-
Q-5	NMA	0.6	18	8	-	-	-
Q-6	NMA	0.6	18	4	-	4	-
Q-7	NMA	0.9	-	-	16	-	-
Q-8	NMA	0.9	-	-	-	-	6

Anhydrides: THPA = Tetrahydrophthalic anhydride
 NMA = Nadic methyl anhydride

R_H = mol anhydride/mol epoxy group

and 3,4-epoxycyclohexylmethyl-3,4-epoxycyclohexane carboxylate (CY-179, Ciba-Geigy).



Curing was performed with nadic anhydride (NMA) and dodecenylsuccinic anhydride (DDSA) at 80, 140, and 180°C with 1 phr of dimethyl benzylamine as catalyst. Curing conditions are summarized in Table 3.

Samples prepared from cycloaliphatic diepoxides at 140° and 180°C contained large bubbles. Very likely under these conditions the curing reaction proceeded too fast and resulted in local overheating.

4.3 Labeled Resin Components

Resin components containing heavy atoms were synthesized for providing centers of high x-ray scattering power at the crosslinks of cured resins. The selected compounds included a brominated anhydride (dibromotetrahydrophthalic anhydride), a tin containing primary diamine [bis(3-aminopropyl)dibutyl tin], and a tin containing diepoxide [dibutyltin-bis(3-propylglycidyl ether)].

Bromine containing anhydrides are commercially available in the form of tetrabromophthalic anhydride and bromomaleic anhydride, but both components were not usable for resin preparations. Because of the high molecular weight of tetrabromophthalic anhydride (MW=464) resin formulations require weight ratios of anhydride to epoxide which exceeded by far the solubility of the anhydride in the epoxide. Blending of both components at elevated temperatures fails due to the high melting point of the anhydride at 275°C. Bromomaleic anhydride is liquid at ambient temperature and can be conveniently blended with epoxides. Unfortunately

Table 3. Epoxy Samples Prepared From Diepoxides by Anhydride Cures at Different Temperatures.

Sample Designation	Epoxy Resin			Anhydride		Hours Cured at		
	6004	CY-178	CY-179	NMA	DDSA	80°C	140°C	180°C
T-1	+			+		26		
T-2		+		+		26		
T-3			+	+		26		
T-4	+				+	26		
T-5		+			+	26		
T-6			+		+	26		
T-7	+			+				6
T-8		+		+				6
T-9			+	+				6
T-10	+				+			6
T-11		+			+			6
T-12			+		+			6
T-13	+			+			12	
T-14		+		+			12	
T-15			+	+			12	
T-16	+				+		12	
T-17		+			+		12	
T-18			+		+		12	

the compound was found to develop acidic fumes during curing due to insufficient temperature stability.

A suitable bromine containing anhydride, dibromotetrahydrophthalic anhydride (DBTHPA), was prepared by bromination of tetrahydrophthalic anhydride (THPA) in chloroform.^{36,37} THPA, recrystallized from toluene, was dissolved in chloroform and a solution of bromine in chloroform was added dropwise under stirring at room temperature until a faint bromine color prevailed for several hours. The precipitated DBTHPA was filtered, washed several times with hexane, and dried. The compound melted at 136-137°C.³⁶ Percent bromine contents determined on three batches (Galbraith Laboratories, Knoxville, Tennessee) were 51.10, 51.05, and 50.93% versus a theoretical value of 51.24%.

Resin formulations containing DBTHPA require handling at elevated temperature (100-110°C) to prevent crystallization of the anhydride. At these temperatures the pot life of the resin is rather short, especially after addition of the tertiary amine catalyst. Unreactive diluents were used to increase anhydride solubility and to extend the pot life of the resin.

For x-ray investigations of epoxy resins prepared by amine cure, a primary diamine containing a tin center was selected. The synthesis of the compound proceeded in three steps:

(1) reduction of dibutyltin dichloride to dibutyltin dihydride³⁸

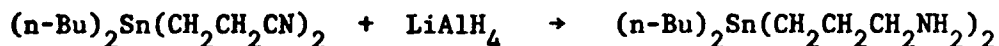


(2) hydrostannylation of acrylonitrile^{39,40}



and

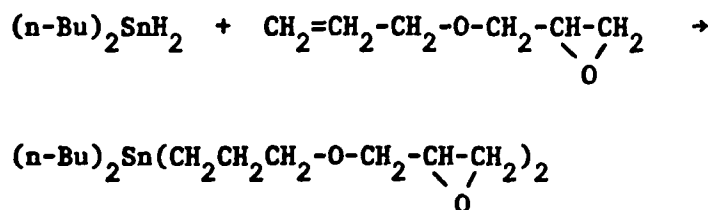
(3) reduction of the dinitrile to the diamine⁴¹



In several preparations the dibutyltin dihydride was obtained with 60-70% yield. The boiling point at 12 mm Hg (1.6 kPa) was 75°C as reported. The yield of dinitrile could be improved by catalyzing the hydrostannylation reaction with a free-radical initiator, azo-bis(isobutyronitrile).⁴⁰ The reaction was monitored by ¹H-NMR spectroscopy for the disappearance of the dihydride. After bulb-to-bulb distillation at 150°C and a pressure of 5×10^{-4} mm Hg (0.07 Pa) a clear, yellow oil was obtained in 50% yield. The ¹H-NMR spectrum in CDCl₃ exhibited the proper ratio of butyl to ethylene protons. The reduction of the dinitrile was carried out in THF. After solvent removal and subsequent bulb-to-bulb distillation a colorless oil was obtained, free of side products according to its 100 MHz ¹H-NMR spectrum.

Several film samples of optimum thickness for x-ray investigations were prepared from Araldite 6004 and the tin containing diamine. The crosslink densities of the cured resins were varied by using a primary monoamine (1-hexylamine) in different amounts as a chain extender. The total concentration of primary amine groups with respect to epoxy groups was kept constant in all formulations (stoichiometric ratio = 1). Resin formulations are summarized in Table 4.

A diepoxide possessing a tin center was prepared by hydrostannylation of allylglycidyl ether.



(I)

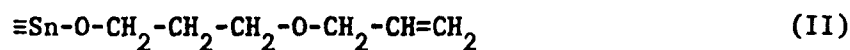
Table 4. Formulations for Araldite 6004 Cured With Dibutyltin-bis(3-aminopropyl)/Hexylamine^a.

Film Designation	Mol Diamine/ Mol Epoxy Resin	Mol Monoamine/ Mol Epoxy Resin	Mol Monoamine/ Mol Diamine
SnDA-3	0.49	-	0
SnDA-4	0.25	0.49	2.0
SnDA-5	0.13	0.73	5.6
SnDA-6	0.064	0.88	13.8
SnDA-7	0.032	0.95	29.7

^a Curing conditions: 3 hrs at 80°C followed by 12 hrs at 120°C.

The reaction was carried out at 50°C in two-fold excess allyl glycidyl ether containing 2 wt-% AlBN. After the excess allylglycidyl ether was removed by distillation at reduced pressure, the residue was bulb-to-bulb distilled at 160°C at 1 μ m Hg.

The $^1\text{H-NMR}$ spectrum of the product after bulb-to-bulb distillation revealed the presence of allyl groups. It was assumed that the hydrostannylation of allylglycidyl ether proceeded in two ways, (i) addition over the allyl group yielding (I), and (ii) addition over the epoxy group whereby allyl ether groups are introduced (II or III).



Reaction (i) proceeds by a free radical mechanism whereas reaction (ii) proceeds ionically. It was anticipated that by increasing the stationary free radical concentration and by keeping the tin dihydride concentration in the reaction medium very low (dropwise addition), reaction (ii) could be sufficiently suppressed. Indeed, under these reaction conditions a product was obtained which, after bulb-to-bulb distillation was found free of allyl groups, at least in amounts detectable by $^1\text{H-NMR}$. A very small signal at 5 ppm indicated the presence of Sn-H bonds, very likely caused by the presence of a trace amount of monoepoxy compound. The compound was not used for the preparation of cured epoxy films.

5.0 X-Ray Scattering

5.1 Interpretation of X-Ray Scattering Data

5.1.1 Desmearing of Slit Collimated X-Ray Scattering Data

In an idealized x-ray experiment, an infinitely thin ray of x-rays impinges upon a sample giving rise (for an isotropic sample) to scattering from the sample which is cylindrically symmetric about the incident beam. This is schematically represented in Figure 4a. The intensity of scattering will vary with scattering angle. Unfortunately, the small angle x-ray scattering from this idealized experiment is infinitesimally small. In order to be able to obtain x-ray scattering which is of sufficient intensity to record, a plane of x-rays, defined by a series of slits, intersects the sample. The intersection of the x-ray beam with the sample is in the form of a line, of finite length and of finite width. The small angle scattering is then recorded in a plane perpendicular to the incident x-ray beam at a distance of about 200 millimeters behind the sample using a counter slit. The counter slit is aligned parallel to the intersection of the incident x-ray beam with the recording plane. The intensity of scattering is recorded as a function of the distance, m , in the recording plane perpendicular to the length of the counter slit.

The shape of the recorded intensity is not identical to that which would occur in the idealized x-ray experiment and is said to be "smeared" with respect to the latter. There are two causes of "smearing". The most obvious is the length of the x-ray beam as it intersects the sample. The other cause is the width of this intersection. At very small values of " m " this can no longer be neglected. A trace of the shape of the incident x-ray beam and the initial recorded scattered x-rays in Figure 4 demonstrate that the breadth of the x-ray beam is non-negligible.

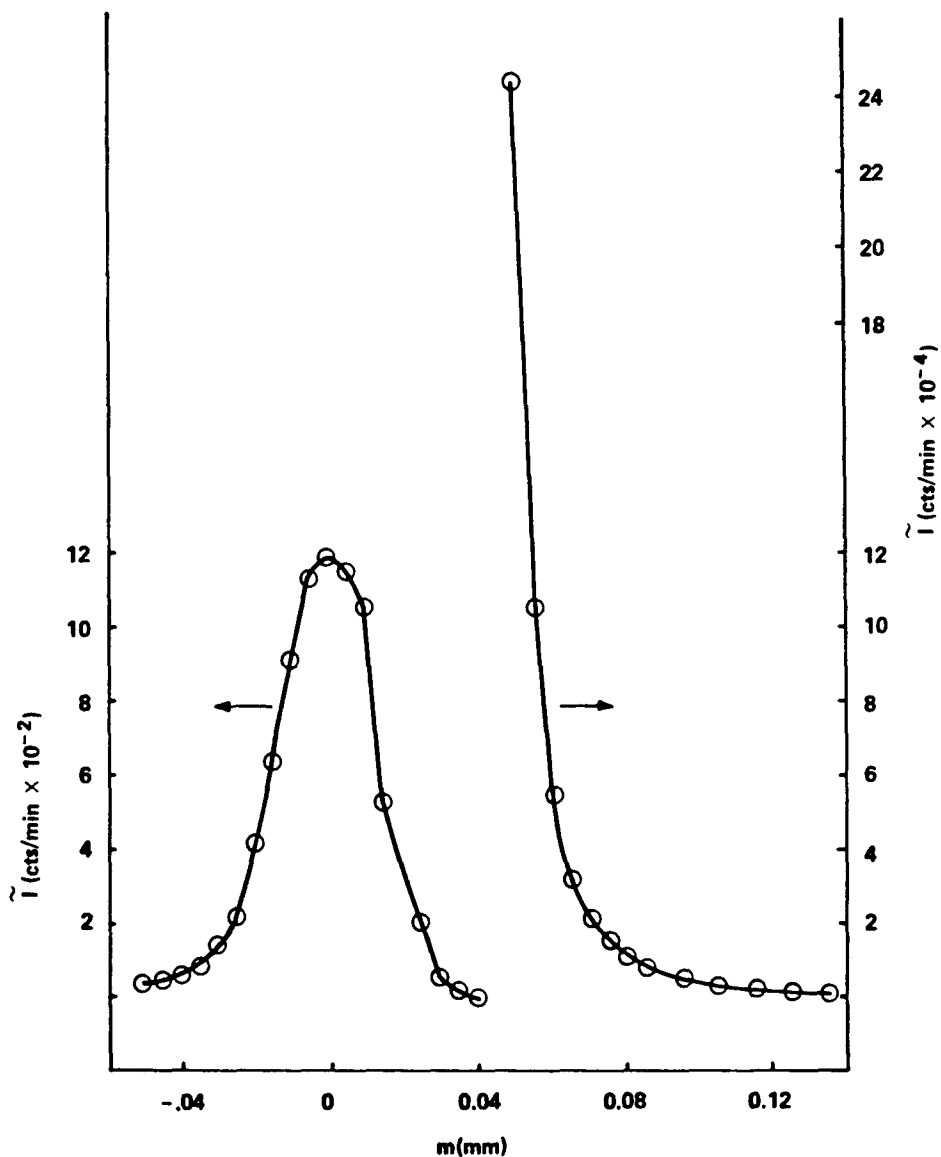


Figure 4. Incident beam profile (left and instrumental scattering (right) plotted versus m (displacement from incident beam profile centroid) for range 1 (see Figure 11). All data is taken with an entrance slit of $15 \mu\text{m}$ and a counter slit of $30 \mu\text{m}$ breadth. The incident beam profile therefore is affected by the breadth of both slits. Incident beam profile is obtained using an absorber.

The methods used to "desmear" the SAXS profile, i.e., to calculate from the actual observed SAXS what the SAXS would be in the idealized experiment are described below. It may be noted that the desmearing for width and length of the x-ray beam may be carried out independently and in any order. Where width desmearing causes a significant change in the SAXS intensity, it must be carried out prior to interpretation. However, certain evaluations of the length smeared SAXS pattern can be made directly without prior desmearing. In the following this possibility will be pointed out, where applicable, with the completely desmeared SAXS intensity distribution, being denoted $I(m)$, the length smeared SAXS intensity given as $\hat{I}(m)$.

5.1.1.1 Correction for Width Smearing

Methods of correcting for width smearing are discussed by Kratky, Porod and Skala.²⁷ The observed intensity at a distance m from the centroid of the incident beam cross-section may be expressed as

$$\hat{I}(m) = \int_{-\infty}^{+\infty} I(m-x)Q(x)dx \quad (1)$$

where the profile of the convolution of the incident beam profile and counter slit profile is given by $Q(x)$ with

$$\int_{-\infty}^{+\infty} Q(x)dx = 1 \quad (2)$$

Equation 1 may be expanded in a Taylor series

$$\begin{aligned} \hat{I}(m) &= \int_{-\infty}^{+\infty} [I(m) - I'(m)x + I''(m)x^2/2 \dots] Q(x)dx \\ &= I(m) - I'(m)\bar{x} + I''(m)\bar{x}^2/2 \end{aligned} \quad (3)$$

As x is measured from the centroid of the beam cross-section (convoluted with counter slit)

$$\int_{-\infty}^{+\infty} Q(x)x dx = \bar{x} = 0 \quad (4)$$

by definition and $\bar{x}^2 = \int_{-\infty}^{\infty} Q(x)x^2 dx$ is the mean square distance from the center of gravity of the beam profile. By setting $I''(m) = \hat{I}''(m)$ we obtain:

$$I(m) = \hat{I}(m) - \hat{I}''(m) \bar{x}^2 / 2 \quad (5)$$

Using Taylor series we obtain:

$$1/2[\hat{I}(m + \sqrt{\bar{x}^2}) + \hat{I}(m - \sqrt{\bar{x}^2})] = \hat{I}(m) + \hat{I}''(m)\bar{x}^2/2 + \dots \quad (6)$$

Combining equations 5 and 6:

$$I(m) = \hat{I}(m) - \frac{1}{2} \{ [\hat{I}(m + \sqrt{\bar{x}^2}) + \hat{I}(m - \sqrt{\bar{x}^2})] - \hat{I}(m) \} \quad (7)$$

Equations 5 and 7 (one or the other) were used to correct the intensity for the beam width effect. Equation 5 was used at the beginning or end of a SAXS run where it is not possible to use equation 7 because no $\hat{I}(\pm \sqrt{\bar{x}^2})$ has been recorded (\pm being read + or -). The required second derivatives were obtained graphically using a plot of $\frac{\Delta \ln I(m)}{\Delta m}$ versus

m using the relationship

$$\frac{d^2 I(m)}{dm^2} = I(m) \left[\frac{d^2 \ln I(m)}{dm^2} + \left(\frac{d \ln I(m)}{dm} \right)^2 \right]$$

5.1.1.2 Correction for Length Smearing

Desmearing of SAXS data obtained from a Kratky camera is required because slits, rather than pinholes, are used to collimate the x-ray beam. The intersection of the x-ray beam with the sample is therefore a line, whereas it would be a point for pinhole collimation. For an isotropic sample, as our crosslinked epoxy resins are, the intensity of scattering will be constant for any given scattering angle. If pinhole collimation is used, and the scattering intensity is registered on a piece of flat film, perpendicular to the x-ray beam, the pattern on that film will be circularly symmetric. The center will be at the intersec-

tion of the x-ray beam with the film and the darkening of the film will be constant for any given radius. If we denote the radial distance by m , and we consider that such a distance is directly related to scattering angle, the quantity we are interested in measuring is $I(m)$, the intensity of scattering as a function of m . Now the intersection of a slit collimated beam with a film perpendicular to the beam is a line. This line may be thought of as a series of points from imaginary pinhole collimated beams strung out along the line. Each of these points will have its own circularly symmetrical scattering pattern associated with it. The patterns from adjacent imaginary pinhole beams are thus superimposed on each other. This situation is illustrated in Figure 5. In Figure 5a an x-ray beam is illustrated scattering from a sample with the scattering pattern registered on a film. The angle of scattering is denoted as 2θ . In Figure 5b, the intersection of a line beam with the film is shown as a straight line. The imaginary point components of this line, A, B, and C, are shown together with circles representing the circularly symmetric scattering associated with point A at a distance r with point B at a distance $r + \Delta r_B$ and with point C at a distance $r + \Delta r_C$. We may represent the observed intensity of scattering from the slit collimated beam as $\tilde{I}(m)$, and the scattering from each point component as $I(m)$. It is seen that the $\tilde{I}(m)$ observed at a distance m from the line contains $I_B[m + (\Delta m)_B]$, $I_C[m + (\Delta m)_C]$ as well as $I_A(m)$. $\tilde{I}(m)$ is described as being slit smeared with respect to $I(m)$. The general expression for $\tilde{I}(m)$ in terms of $I(m)$ is given as

$$\tilde{I}(m) = \int_{-\infty}^{\infty} P(t) I(\sqrt{m^2 + t^2}) dt \quad (4)$$

where $P(t)$ is a weighting function which depends on the distribution of intensity along the line shown in Figure 5. In general, the intensity

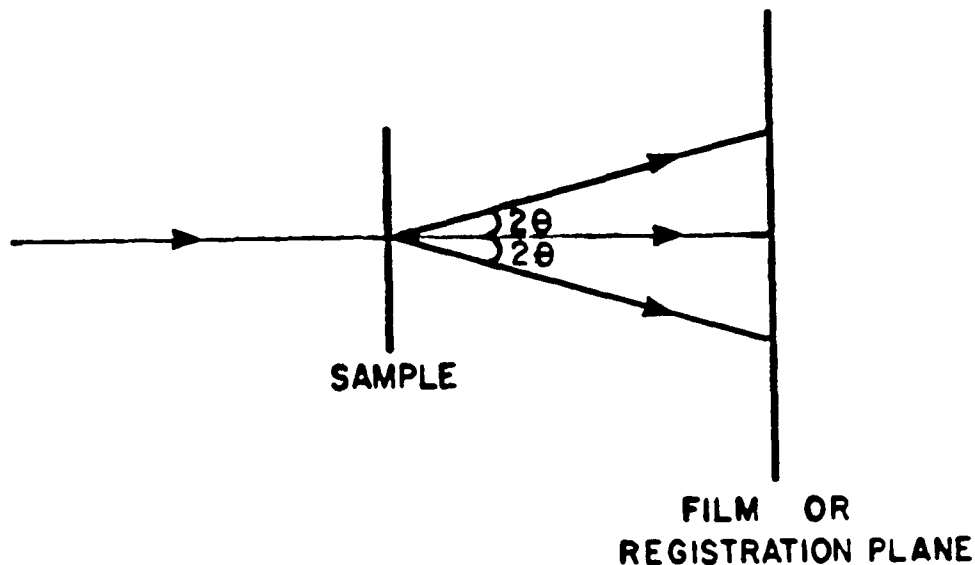


Figure 5a. Schematic representation of the x-ray scattering experiment.

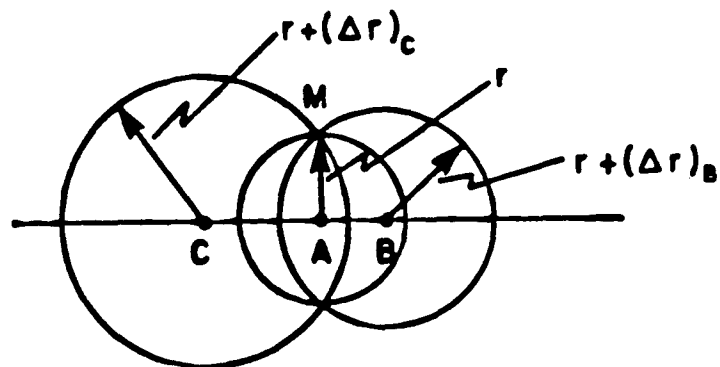


Figure 5b. Intersection of the scattered x-rays with the registration plane for a slit collimated beam. The line beam may be thought of as composed of many points, lined side by side. Three of these points are designated A, B, C. Portions of the cylindrically symmetrical scattering pattern for each point are shown intersecting at point M.

distribution along the beam will be trapezoidal as shown in Figure 6. If the length of the top part of the trapezoid (representing constant intensity) exceeds the m at which $\tilde{I}(m)$ is negligible, the beam may be considered infinite, and $P(t) = 1$ in equation 4. In terms of Figure 6 an infinitely long beam is one for which $(\ell-k) > m$ for the smallest m above which $\tilde{I}(m) = 0$. It is assumed that $\tilde{I}(m)$ is measured at a point corresponding to the center of the trapezoidal distribution with a slit of infinitely small lateral extent. Since, in general, a slit of some lateral extent, $2z$, is used, the condition for an infinite beam is $(\ell-k-z) > m$ for the smallest m above which $\tilde{I}(m) = 0$. We will see later that this condition may be modified slightly if the trapezoidal distribution adheres to certain conditions.

The process of obtaining the intensity distribution $I(m)$ from the observed intensity distribution $\tilde{I}(m)$ is referred to as desmearing.

5.1.1.3 Desmearing for an Infinite Beam

For an infinite beam equation 4 may be rewritten as

$$\tilde{I}(m) = 2 \int_0^{\infty} I(\sqrt{m^2 + t^2}) dt \quad (5)$$

Guinier and Fournet^{27,41,42} and du Mond^{27,42,43} showed that this could be desmeared in the following way: The derivative of the observed intensity distribution is obtained and divided by m . This quantity is called $F(m)$. It can then be shown that $I(m)$ is proportional to the smeared $F(m)$, i.e., to $\tilde{F}(m)$

$$I(m) = \frac{1}{2\pi} \tilde{F}(m) = \frac{1}{\pi} \int_0^{\infty} F(\sqrt{m^2 + s^2}) ds \quad (6)$$

5.1.1.4 Desmearing for a Finite Beam

For a finite beam desmearing may be carried out by a modification of equation 6, provided that the intensity distribution along the beam satisfies the following criterion. The shape of the symmetrical trape-

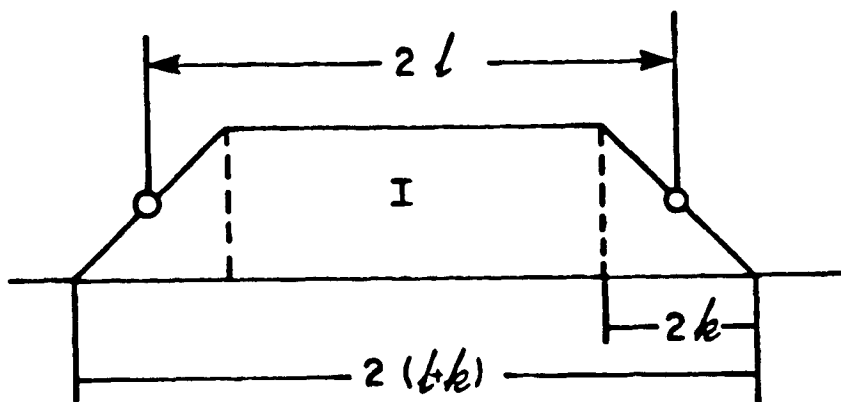


Figure 6 Typical Kratky camera incident beam profile at registration plane.

zoid must be such that $k/l = 0.4^{27,44}$ (see Figure 6). When a counter slit of finite length is used the effective trapezoidal shape is modified by the length (lateral extent) of the counter slit. If $2k$ of the beam profile and $2z$, the length of the counter slit, are similar in magnitude with $z > k$, then the effective width of the shoulder of the trapezoid, $2\bar{k}$, is given as

$$2\bar{k} = 2z + 2k/3 \quad (7)$$

If $\frac{2\bar{k}}{2l} = \frac{2k + 2k/3}{2l} = 0.4$, then the equation for desmearing becomes²⁷

$$I(m) = \frac{1}{\pi} \int_0^{\ell-k} F(\sqrt{m^2 + s^2}) ds + \frac{1}{2\ell} \tilde{I}(\sqrt{m^2 + (\ell-\bar{k})^2}) \quad (8)$$

This may be recognized as a modification of equation 6. It may also be noted that when $\tilde{I}(m) = 0$ for $m > (\ell - \bar{k})$ the x-ray beam length is effectively infinite and equation 8 reduces to equation 5.

5.1.1.5 Slit Length Desmearing at RTI Using the Spline Function Approximation of the Scattering Curve for Numerical Differentiation.

The desmearing is accomplished by a computer program described by Heine and Roppert^{45,46}. It was acquired courtesy of Prof. W. Krigbaum at Duke University and adapted for use at RTI. The derivatives required (see Equation 6) are obtained by use of a spline function as described below. In all data processing the infinite beam approximation was valid.

5.1.1.6 Spline Function Approximation of Scattering Curve for Numerical Differentiation

The computer program for the desmearing process requires the derivative of the observed intensity distribution $d\tilde{I}(m)/dm = \tilde{I}'$. Graphical differentiation can be subjected to considerable errors especially in

the case of steeply descending functions. For this reason, the experimental intensity data are interpolated by a collocation spline function which supplies the required derivative of the intensity distribution.

The experimental scattering intensities are plotted vs reciprocal Bragg distances and a smooth curve is drawn by visual inspection. Points (knots) are then selected on the curve which define the interpolating spline function. The spline function as well as its first derivative are then calculated.

Further improvement of the evaluation method was obtained by a change to a natural spline for interpolation. The first spline approximation⁴⁷ required the slopes at the boundaries of the interpolation interval to be known since they are input parameters. Especially the initial slope at small scattering angle is difficult to estimate, and, consequently, errors might be introduced in the initial part of the intensity distribution. The boundary conditions for a natural spline are given by the second derivatives of the spline being zero at the boundaries, i.e., the spline starts and ends without curvature. The first derivatives at the boundaries follow from the general continuity conditions.⁴⁸

The first derivatives y'_i at the knots x_i, y_i of a natural spline are defined by the equation system where h_i denotes $x_{i+1} - x_i$. The

$$\begin{bmatrix} \frac{2}{h_1} & \frac{1}{h_1} & & & \\ \frac{1}{h_1} & 2\left(\frac{1}{h_1} + \frac{1}{h_2}\right) & \frac{1}{h_2} & & \\ & \frac{1}{h_{i-1}} & 2\left(\frac{1}{h_{i-1}} + \frac{1}{h_i}\right) & \frac{1}{h_i} & \\ \dots & \dots & \dots & \dots & \\ & & & \frac{1}{h_{n-1}} & \frac{2}{h_{n-1}} \end{bmatrix} \begin{matrix} y'_1 \\ y'_2 \\ y'_i \\ \dots \\ y'_n \end{matrix} = \begin{bmatrix} \frac{3}{h_1^2} (y_2 - y_1) \\ \dots \\ 3 \left[\frac{y_{i+1} - y_i}{h_i^2} + \frac{y_i - y_{i-1}}{h_{i-1}^2} \right] \\ \dots \\ \frac{3}{h_{n-1}^2} (y_n - y_{n-1}) \end{bmatrix}$$

parameters for the cubic of the interpolation interval h_i are then derived from the equation system

$$\begin{bmatrix} 1 & x_i & x_i^2 & x_i^3 \\ 1 & x_{i+1} & x_{i+1}^2 & x_{i+1}^3 \\ 0 & 1 & 2x_i & 3x_i^2 \\ 0 & 1 & 2x_{i+1} & 3x_{i+1}^2 \end{bmatrix} \begin{matrix} a \\ b \\ c \\ d \end{matrix} = \begin{bmatrix} y_i \\ y_{i+1} \\ y'_i \\ y'_{i+1} \end{bmatrix}$$

The ordinate for the interpolated point $x_i < x < x_{i+1}$ is then given by

$$y = a + bx + cx^2 + dx^3 \quad (9)$$

The first derivative of the intensity distribution at x is given by

$$y' = b + 2cx + dx^2 \quad (10)$$

Although spline approximations are extremely well suited to representing functions which cannot be expressed in closed form and for obtaining their first derivatives, care has to be taken in the selection of the knots. Inside an interpolation interval the first derivative is given by Equation 10. If the intervals are taken too large, long segments of the derivative will follow a second order parabola, thus introducing an artifact in subsequent data manipulation. If the intervals are taken too closely spaced, reading errors become significant which show as weak undulation of the approximating spline around the actual curve. This undulation can be so weak that it remains unobservable on the spline but it becomes very pronounced in its first derivative. In order to avoid such possible pitfalls, the angular dependence of the calculated first derivatives is always checked graphically for smoothness.

As seen later, the intensity of scattering at the tail end of the curve should be constant when multiplied by m^4 [i.e., $m^4 I(m) = \text{constant}$]. It was found that the spline function can induce a significant fluctuation in $m^4 I(m)$ varying smoothly with m but not justified by the actual data. Fortunately there is a check for this because $m^3 I(m)$ should also be constant.

5.1.2 Information Attainable From SAXS

Small angle x-ray scattering (SAXS) of solid materials is often used for semi-crystalline samples to detect repeat distances between regularly spaced lamella. This is manifested by a peak in the graph of scattered x-ray intensity versus scattering angle. For cured epoxy samples no regularly spaced alterations of electron density with repeat distances in the range 30-1000 Å are anticipated and a broad SAXS peak has been observed in only one instance (see Section 5.2.5.2).

However, SAXS is additionally capable of providing information concerning the mean density fluctuation within a sample. If we assume that such density fluctuations find their origin in two phases, each of uniform electron density caused by different degrees of crosslinking, the method can be interpreted in terms of the density difference between the two phases assuming each phase makes up 50% of the sample. In addition, the relative size of such uniform phases may be obtained as well as information relating to the actual electron density fluctuations within each phase, i.e., to what extent the assumption that each phase is of uniform electron density is actually valid. The conventional methods of extracting this data from the SAXS intensity distribution are described below.

5.1.3 Angular Nomenclature

The angle between the incident and scattered beam is designated as 2θ . In the following discussion of the interpretation of x-ray scattering, material is drawn from a variety of sources. Unfortunately, three principal angular functions are used for consistency with the original literature.⁴⁹ These are, for small angles

$$\begin{aligned} s &= \frac{2\theta}{\lambda} \\ h &= \frac{4\pi\theta}{\lambda} \\ m &= 2a\theta = a\lambda s \end{aligned} \quad (11)$$

where m is the linear distance between the scattered and incident rays in the plan of registration of the Kratky camera, a is the distance between sample and the plane of registration (normally 205 mm) and λ is the wavelength of the incident x-rays (1.542 Å).

5.1.4 Guinier Plot

Guinier's treatment of SAXS scattered intensity yields a dimension for particles of electron density, differing from the mean electron density of the sample, for the case where inter-particle interference is negligible. It is routinely used for determining the size of polymer molecules in dilute solution. In the following we explain the basis of this treatment for a system of homodisperse particles in dilute solution and then examine the effect of polydispersity and interparticle scattering, which must be considered for epoxy samples.

As x-rays impinge on a particle the electrons in that particle are forced into oscillation by the electromagnetic field of the x-rays. The electrons in turn become a source of radiation, and in this way, the electrons are said to scatter the impinging radiation. When the angle between the incident and scattered radiation is 0° , all the scattered

radiation interferes constructively. But for all other angles some degree of destructive interference is inevitable, as the path length traversed by incident + scattered beam from one electron in the particle will, in general, be different from that scattered by another electron in the same particle. Thus, the atomic scattering factor, f , the scattering by an isolated atom is proportional to the atomic number at zero scattering angle, but decreases with angle as shown in Figure 7. It is intuitively obvious that as the scattering particle increases in size, the peak at 0° will become sharper, and the shape of the curve will become steeper. Debye⁵⁰ showed that for an isolated particle for which the scattering is averaged over all possible orientations with the respect to the incident x-ray beam, the intensity of scattering may be expressed:

$$I(h) = \overline{F^2(h)} = \sum_{j=1}^m \sum_{k=1}^m f_j f_k \frac{\sin(h r_{jk})}{h r_{jk}} \quad (12)$$

Here $h = \frac{4 \pi \sin \theta}{\lambda}$ where 2θ is the scattering angle (the angle between incident and scattered x-rays), λ is the wavelength of the incident radiation, f_j is the atomic scattering factor of the j th atom and r_{jk} is the distance in the particle between the j th and k th atom. Guinier⁵¹ recast equation (12) as

$$\overline{F^2(h)} = \left(\sum_{j=1}^m f_j \right)^2 - \frac{(h^2)}{6} \sum_{j=1}^m \sum_{k=1}^m f_j f_k r_{jk}^2 + \dots \quad (13)$$

$j \neq k$

by expressing $\sin \chi / \chi$ as the power series $1 - \chi^2/6 + \dots$ and retaining only the first two terms. By defining the electronic center of gravity, o , by $\sum f_j \vec{r}_{oj} = 0$ and expressing equation (2) in terms of \vec{r}_{oj} , he showed

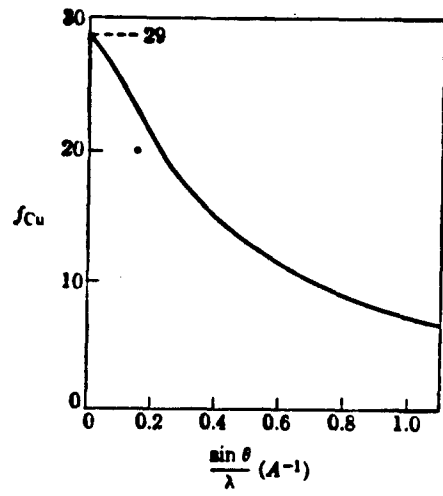


Figure 7. The atomic scattering factor of copper.

that

$$\overline{F^2(h)} = \left(\sum_j f_j\right)^2 \left[1 - \frac{h^2 \sum_j f_j r_{oj}^2}{3 \sum_j f_j} + \dots\right] \quad (14)$$

Since the term $\frac{\sum_j f_j r_{oj}^2}{\sum_j f_j} = R^2$, R being the electronic radius of gyration, and the term in brackets is the power series expansion of an exponential function, the Guinier approximation is given as:

$$I(h) = \overline{F^2(h)} = \left(\sum_j f_j\right)^2 e^{-\frac{h^2 R^2}{3}} \quad (15)$$

Thus one can obtain the radius of gyration, R, of a particle from the initial slope of the Guinier plot, $\ln I(h)$ vs h^2 .

One can obtain further information concerning the shape of the particle from Guinier plots in which $\ln h I(h)$ or $\ln h^2 I(h)$ are plotted versus h^2 . Such plots would be linear (at scattering angles higher than those used for the initial slope) for rods or plate-like particles respectively. But as a spherical shape would appear to be the best assumption for the type of particle to be expected in a cured epoxy resin and polydispersity and interparticle interferences would preclude such detailed analysis in any case, no effort has been made to analyze the data in this way.

The radius of gyration must be obtained from data near the origin of the $\ln I$ vs h^2 plot. It is necessary to define the point at which the $\ln I$ versus h^2 plot will deviate significantly from that predicted by Guinier's law. For spherical particles⁵² Guinier's approximation is an accurate presentation of the scattering curve up to $h \cdot R = 1.3$, after which the actual curve falls below that predicted by Guinier's approximation. For rod like particles Guinier's approximation is a good approximation up to $hR = 0.7$, after which the actual curve rises above that

predicted by Guinier's approximation. Particles which are in the shape of an ellipse would be intermediate between these two and if the major and minor axes differ only slightly, the Guinier approximation would be good to scattering angles somewhat higher than $hR = 1.3$

5.1.4.1 Effect of Polydispersity

The radius of gyration, as obtained from the Guinier plot, tends to favor the largest particles heavily.⁵³ When expressed in terms of $m(R_o) dR_o$, which gives the total mass of particles whose radius of gyration is contained between R_o and $R_o + dR_o$, the mean observed radius of gyration, R_{om} is given as:

$$R_{om}^2 = \frac{\int m(R_o) R_o^5 dR_o}{\int m(R_o) R_o^3 dR_o} \quad (16)$$

5.1.4.2 Effect of Interparticle Interference

For particles of uniform size, interparticle interference causes the initial part of the $I(h)$ versus (h) curve to decrease and therefore decreases the slope of curve close to the incident beam. This effect is the more pronounced the higher the concentration of particles. For a heterogeneous mixture of particles the deviations from the scattering phenomena calculated for isolated particles is less marked. In fact, Guinier and Fournet state:⁵⁴ "in a mixture of non-identical particles of arbitrary forms and with random distribution (no long-range order) it is improbable that the packing of particles will lead to large changes in the scattering curves and that thus the laws for widely separated particles can furnish the orders of magnitude of the scattering phenomena".

5.1.5 The Invariant and Scattering Power of the Sample

The mean square fluctuation of electron density $\overline{(\rho-\bar{\rho})^2}$ is the only quantity that can be obtained from the small angle x-ray scattering data, without assumptions concerning the nature of the inhomogeneities. The quantity, $\overline{(\rho-\bar{\rho})^2}$ is called the scattering power of the sample and may be obtained from absolute intensity data by means of the relations:^{49,55}

$$\overline{(\rho-\bar{\rho})^2} = \frac{1}{P_0} \frac{4\pi}{i N^2} \frac{1}{da\lambda^3} \int_0^{\infty} m^2 I(m) dm. \quad (17)$$

Absolute intensity data means that the ratio of scattered intensity to the intensity of the incident x-ray beam is known. This ratio is routinely obtained for our samples by measuring the intensity of scattering of a standard Lupolen sample at 150 Å which has been calibrated⁵⁶ so that the ratio of the measured scattering intensity to the intensity of the incident beam is known. In equation 18

m = distance between the incident and scattered rays in the plane of registration in centimeters.

a = specimen to registration plane distance, normally 20.5 cm for the Kratky camera.

d = specimen thickness in centimeters

λ = wavelength of the x-rays, for CuK_α , 1.5418×10^{-8} cm.

$i_e = 7.9 \times 10^{-26}$, the Thomson scattering constant of a free electron

N = Avogadro's number

P_0 = Intensity of the incident x-ray beam

Equation 18 assumes that the data has been obtained using pinhole collimation or has been desmeared. Slit smeared data may be used without

desmearing using the relation:

$$\frac{1}{(\rho-\bar{\rho})^2} = \frac{1}{P_0} \frac{2\pi}{i_e N^2} \frac{1}{d\lambda^3} \int_m \tilde{I}(m) dm \quad (18)$$

This differs from equation 18 in that m , rather than m^2 , is included in the integral and the integral is multiplied by a factor half of that used in equation 18. The integrals in equation 18 and 19, have been called the invariant by Porod⁵⁷ and are designated by the symbols:

$$\begin{aligned} Q_m &= \int_0^\infty m^2 I(m) dm \\ \tilde{Q}_m &= \int_0^\infty m \tilde{I}(m) dm \end{aligned} \quad (19)$$

These quantities will depend only on the scattering power of the sample and will be unaffected by the size of domains of uniform electron density as long as the size is large enough (greater than 100 Å) to yield scattering in the small angle region.

If one assumes that a specimen may be approximated by a two-phase model, each of uniform electron density, then the scattering power is given by

$$\frac{1}{(\rho-\bar{\rho})^2} = (\rho_1 - \rho_2)^2 W_1 W_2 \quad (20)$$

where ρ_1 and ρ_2 are the electron densities of the two phases, and W_1 and W_2 , the respective volume fractions.

5.1.6 Determination of the Invariant, the Specific Surface, and Uniformity of Electron Density Over Small Distance

As seen by Equation 20, determination of the invariant requires knowledge of the function $m^2 I(m)$ or $m \tilde{I}(m)$ at a scattering angle close to zero, where data cannot be obtained because of the presence of the incident x-ray beam and at large angles where the scattered intensity is too weak to measure accurately. Errors in approximations made for the scattered intensity close to the incident beam will not affect the

invariant greatly because of weighting by m or m^2 but by the same token, errors at large angles will be very important.

If data is obtained to small enough angles, it is found that the curve of I_m^2 or \tilde{I}_m begins to decrease with decreasing angle and an extrapolation to $m = 0$ is possible. This allows estimation of the quantity \tilde{I}_m or I_m^2 at scattering angles smaller than those experimentally attainable. The scattering intensity at very high angles can be obtained by using the theoretical finding that $h^4 I = k$ in the high angle region as discussed in the next section.

5.1.7 The Correlation Function, Specific Volume, Transversal Lengths and Correlation Distance

The correlation function $\gamma(r)$ has been defined as follows by Debye et al⁵⁸ as well as by Porod,⁵⁷ who refers to it as the characteristic:

$$\gamma(r) = \frac{(\Delta \rho)_1 \cdot (\Delta \rho)_2}{(\Delta \rho)^2} \quad (21)$$

Here $(\Delta \rho)_1$ and $(\Delta \rho)_2$ are the local fluctuations of electron density at points 1 and 2, separated by the distance, r , from the average electron density, $\bar{\rho}$, and $\overline{(\Delta \rho)^2}$ is the average value of the square of such fluctuations. This function will vary from 0 when r is very large to 1 when $r = 0$. It is related to the intensity of scattered radiation by Fourier transformation:⁵⁷

$$I(h) = 4\pi \int_0^\infty \gamma(r) r^2 \frac{\sin hr}{hr} dr \quad (22)$$

$$\gamma(r) = \frac{1}{2\pi^2} \int_0^\infty h^2 I(h) \frac{\sin hr}{hr} dh \quad (23)$$

The relationship existing between $I(h)$ and $\gamma(r)$ is therefore analogous

to the one which exists between the Patterson function and the distribution of (hkl) intensities of conventional crystal structure analysis.

For an isolated particle, $\gamma_0(r)$, the correlation function of the isolated particle is given by the expression:

$$\gamma_0(r) = \frac{\bar{V}(r)}{V} \quad (24)$$

Here $\bar{V}(r)$ is the average volume common to the particle and an identical particle (its ghost) displaced by the vector r for all directions of the vector. The volume common to a particle and its ghost is shown for one direction of the vector, in Figure 8.

If we begin at any arbitrary point within the particle, and lay down a ruler of length r in any direction, then $\gamma_0(r)$ also expresses the probability that the other end of the ruler will also fall within the particle. The function $\gamma_0(r)$ is plotted as a function of r for a sphere of radius, R , in Figure 9.

For any two phase system, it can be shown that the slope of the characteristic at $r = 0$ is given:

$$\left(\frac{d\gamma}{dr}\right)_{r=0} = \frac{1}{4c(1-c)} \frac{S}{V} \quad (25)$$

where V is the volume of the phase of volume fraction, c , and S is the surface area between the two phases. From the definition of $\gamma(r)$, equation 22, it is clear that $\gamma(0) = 1$. However, the greater the surface to volume ratio (the specific surface, S/V), the greater the probability that "rulers" of r close to zero will lie with one end in one phase and the other in the other phase. Each "ruler" with ends in different phases contributes zero to $\gamma(r)$, hence contributing to the decrease of $\gamma(r)$ with r close to $= 0$.

The specific surface can be obtained from the part of the small angle scattering curve at high angles. This follows from the fact that

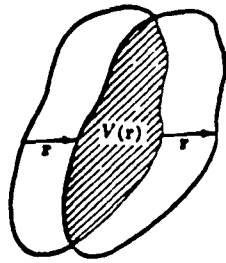


Figure 8. A representation of the function of $\bar{V}(r)$.

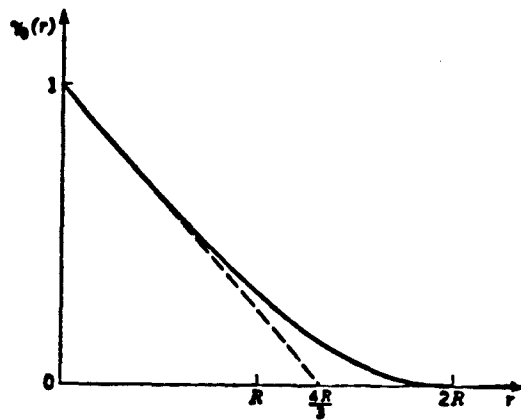


Figure 9. The function $\gamma_0(r)$ for the sphere of radius R .



Figure 10: Physical concept of the transversal length.

since $hI(h)$ and $r\gamma(r)$ are related by a Fourier transform (see Equations 23 and 24), the high angle part of the curve of $I(h)$ corresponds to the part of the curve of $\gamma(r)$ at small values of r . It can be shown^{57,58} that as a consequence of this

$$h^4 I(h) = k \quad (26)$$

for pinhole collimation or for a desmeared curve and

$$h^3 \tilde{I} = k_1 \quad (27)$$

for a smeared intensity distribution. The specific surface can then be obtained from the relationship

$$S/V = \frac{2\pi^2}{\gamma a} W_1 W_2 \frac{k}{Q} \quad (28)$$

or

$$S/V = \frac{8\pi}{\lambda a} W_1 W_2 \frac{k_1}{\tilde{Q}} \quad (29)$$

where a is the sample to registration plane distance, W_1 is the volume fraction of one phase, W_2 that for the other phase, and Q (or \tilde{Q}) is the invariant as defined by Equation 20.

For an irregular two-phase system of phases 1 and 2 the specific surface may be related to transversal lengths as illustrated in Figure 10. The average intersection of arrows (in all directions) with each phase are given by:

$$\bar{l}_1 = \frac{4 W_1}{S/V} \quad (30)$$

$$\bar{l}_2 = \frac{4 W_2}{S/V} \quad (31)$$

where W is the volume fraction of each phase.

A correlation distance, \bar{l}_c , may be defined:

$$\text{for which } \frac{1}{\bar{l}_c} = \frac{1}{\bar{l}_1} + \frac{1}{\bar{l}_2} \quad (33)$$

$$\text{and } S/V = \frac{4 W_1 W_2}{\bar{l}_c} \quad (34)$$

Consideration of Equation 34 reveals that $\bar{\ell}_c$, the correlation distance, is always smaller than $\bar{\ell}_1$ or $\bar{\ell}_2$. The quantity, $\bar{\ell}_c$, is obtained directly from the SAXS data without any additional information. For cases where $\bar{\ell}_1$ is very much smaller than $\bar{\ell}_2$ (W_1 much smaller than W_2) $\bar{\ell}_c$ is approximately equal to (slightly smaller than) $\bar{\ell}_1$.

In practice, the high angle region of the small angle scattering curve will usually be given by an expression of the type:

$$\tilde{I}(h) = \frac{k_1}{h^3} + k_2 \quad (37)$$

rather than by Equation 27. The additional term k_2 is caused by fluctuations of electron density at small distances⁵⁹ (deviations from the assumption that each phase is of uniform electron density). Such a term is particularly noticeable for slit smeared data because the smearing is caused by the addition of higher angle intensity data to a given $I(h)$ (see Equation 4).

Additionally, the assumption is made that the transition from one phase to the other is sharp in the derivation of Equations 27 and 28. A zone of gradual transition would tend to decrease the observed k or k_1 . Methods for estimating the size of the zone of gradual transition between phases, as well as accurate determination of k_2 (equation 38) and S/V (Equations 29 and 30) are discussed by Ruland.⁶⁰

The correlation distance, $\bar{\ell}_c$, can also be obtained from the SAXS intensity profile close to the main beam. Debye, Anderson and Brumberger⁵⁸ have shown that for a random distribution of two phases

$$\gamma(r) = \exp \frac{-r}{\bar{\ell}_c} \quad (32)$$

the intensity of scattering for such a random two-phase system is given

as:

$$I(h) = \frac{A}{(1 + h^2 \bar{\ell}_c^2)^2} \quad (35)$$

A plot of $[I(h)]^{-1/2}$ versus h^2 should yield a straight line whose slope-intercept ratio would yield $\bar{\ell}_c$

$$\bar{\ell}_c = \frac{\lambda}{2\pi} \left(\frac{\text{slope}}{\text{intercept}} \right)^{1/2} \quad (36)$$

For slit smeared intensities

$$\tilde{I}(h) = \frac{A}{(1 + h^2 \bar{\ell}_c^2)^{3/2}}$$

and $\bar{\ell}_c$ may be obtained using equation 36 and a plot of $\tilde{I}(h)^{-2/3}$ versus h^2 .⁶¹

5.1.8 Swelling Sample as a Means of Modifying SAXS

As SAXS is sensitive to electron density variation within a sample, the changes that occur in the SAXS of a sample after swelling can yield useful information. For example, where SAXS is caused by voids accessible to a solvent, the SAXS would be largely wiped out by when solvent fills the voids. Where a lightly cross-linked region differs little in density from a tightly cross-linked zone, but is much more accessible to solvent, permeation of heavy atom containing solvent might increase SAXS due to an increase in electron density contrast. The same effect might be obtained if it were possible to react a heavy atom containing curing agent with a tetrafunctional epoxy molecule only after the first two functions are satisfied, i.e., only when epoxy molecule is involved in cross-linking.

5.1.9 Application of Heavy Atom Tagging to Spatial

Distribution of Cross-links

The method of elucidating the spatial distribution of cross-links by heavy atom tagging requires that two conditions be fulfilled. Firstly, the heavy atoms must be identified with cross-links and not be present in parts of the network in which not all functionalities of the epoxy or

hardener molecules are satisfied leading to non-cross-linked chains. Secondly, interference from scattering by non-heavy atom components must be accounted for. This is particularly important for epoxy networks for which cross-links are so closely spaced that the distances between them would be expected to fall in the range of 5-15 Å.

This is seen on consideration of the equation for the scattering from an isotopic sample

$$I(s) = \sum_n \sum_m f_m f_n \frac{\sin(sr_{mn})}{sr_{mn}} \quad (38)$$

where f_m and f_n are the atomic scattering factors of the m th and n th atoms and r_{mn} is their separation. The heavy atom method works because the atomic scattering factor is much larger for the heavy atoms than for lighter atoms such as carbon, oxygen and nitrogen. If we use the subscript L for the light atoms and H for heavy atoms, the vector r_{HH} is weighted to a considerably greater extent in Equation 39 than r_{LL} or r_{LH} . However, in the range of 5-15 Å this advantage is overcome to some extent by the fact that the number of light atoms is greater than that of the heavy atoms and they tend to distribute themselves in such a fashion that certain values of r_{LL} occur with great frequency. This leads to peaks in the SAXS pattern for epoxy resins (containing no heavy atoms) with Bragg values corresponding to approximately the most favored value of r_{LL} . It then becomes necessary to devise a second sample which will have the same r_{LL} and r_{LH} distribution as the sample of interest so that only the r_{HH} distribution differs. The desired information concerning the distribution of r_{HH} can then be obtained by subtracting the SAXS pattern of the second sample from that of the first. Such schemes have been applied by Brady et al^{62,63} and Li, Post and Morawetz⁶⁴ to heavy

atom tagged polymeric molecules in solution. Brady subtracted the x-ray scattering pattern of heavy atom labeled monomer in solution from that of heavy atom labeled polymer in solution. Li, Post and Morawetz⁶¹ used the scattering from solutions of oligomers tagged at both ends with iodine. The L-H interactions in the molecule and with the solvent were corrected for by subtracting the x-ray scattering from solutions of the corresponding oligomer tagged at only one end, yielding the end to end distance in the diiodo-oligomer.

5.2 Results of X-Ray Scattering Measurements From Cured Epoxy Samples

5.2.1 Introduction

The strategy in obtaining small angle x-ray scattering data has been to select several series of samples in which trends might be expected to be followed from sample to sample, concerning the sizes of highly cross-linked clusters. Each series consisted of samples cured at progressively higher temperatures. SAXS measurements made in the first year of the investigation revealed that the most intense small angle x-ray scattering from the sample was occurring at extremely small angles. This observation was in accord with the results of SAXS investigations by other investigators both on cured epoxy samples and for other amorphous polymers. Efforts were therefore directed at obtaining SAXS data at the smallest possible scattering angle.

The low scattering power of the samples raised the possibility that the scattering was originating exclusively at the sample surfaces. The sample had been prepared on glass plates coated with Frekote to prevent adhesion of the epoxy to the glass surface. This produce samples with "cloudy" surfaces. Absolutely clear samples could be prepared by coating the glass plates with a fluorine-rich plasma polymer film. The SAXS of

such samples was measured towards the end of the investigation and found to yield no distinctive features; the SAXS intensity distribution was independent of angle. This suggests that the intensity peak at very small angles obtained for samples prepared on Frekote coated plates was caused by Frekote or Frekote induced modifications at the surface of the samples.

Where such strong intensity at very small angles was found, the scattering power and correlation length were obtained. For the latter both the Debye method (Equation 36) and Porod method (Equation 26) were used. Diffuse scattering from cured epoxy samples was observed at very small angles. Accurate SAXS data was therefore obtained as close as possible to the main beam. SAXS data were routinely obtained at displacements (in the registration plane) from the incident beam centroid of $60 \mu\text{m}$, corresponding to a Bragg spacing of 5000 \AA . This involves the use of extremely narrow entrance slits ($15 \mu\text{m}$), counter slits ($30 \mu\text{m}$) and careful alignment of the Kratky camera.

The protocol used to collect SAXS data is illustrated in the log-log plot shown in Figure 11. It involves four combinations of entrance and counter slits with broader slits used to register the less intense scattering at the higher angles. The registration of scattering by scanning over the two lowest ranges of scattering angles was added in the second year and accomplished using a graphite crystal monochromator on Kratky camera 2. Registration of scattering data for the two highest ranges of scattering angles is accomplished using Kratky camera 1. The use of two counter Kratky cameras reduces the amount of camera alignment needed to collect the data.

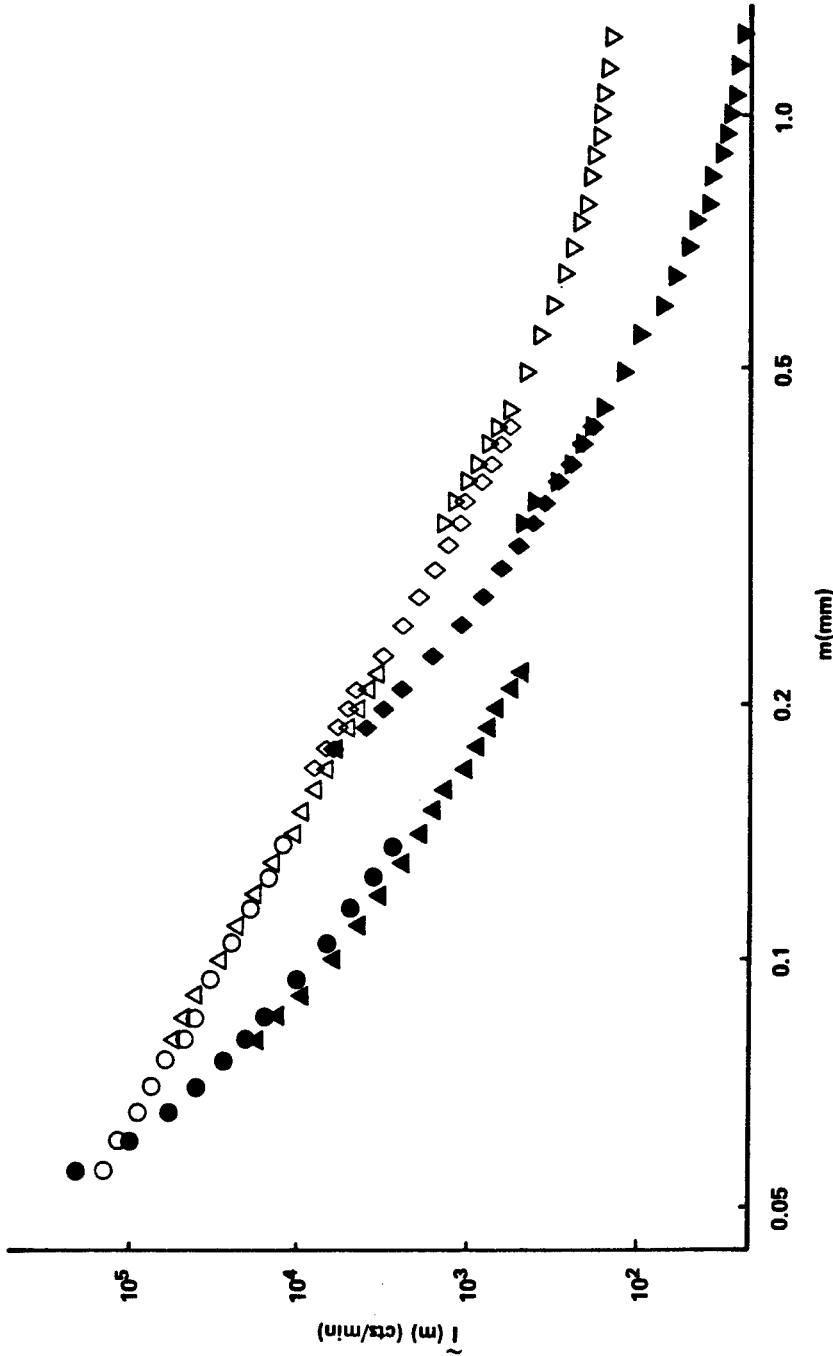


Figure 11. Plot of $\log I$ versus $\log m$ (I = scattered intensity, m = displacement of counter slit from the incident beam centroid in the registration plane of the Kratky camera). Filled symbols represent sample scattering (obtained by subtracting instrumental scattering from sample + instrumental scattering). Data was obtained over four ranges of scattering angles with the following combination of entrance (E) and counter (C) slits.

- o Range 1, $m = 0.041$ mm to 0.136 mm, E - $15 \mu\text{m}$, C = $30 \mu\text{m}$
- Δ Range 2, $m = 0.08$ mm to 0.22 mm, E - $20 \mu\text{m}$, C = $30 \mu\text{m}$
- \diamond Range 3, $m = 0.17$ mm to 0.43 mm, E - $40 \mu\text{m}$, C = $50 \mu\text{m}$
- ∇ Range 4, $m = 0.33$ mm to 0.71 mm, E = $40 \mu\text{m}$, C = $200 \mu\text{m}$

(The tail end of this range is not shown in the graph as there is very little change of I with m).

5.2.2 Experimental Results

5.2.2.1 Protocol for Collection of SAXS DATA for Cured

Epoxy Samples

SAXS data was obtained using a Kratky camera with a 40 μm entrance slit and a 100 μm or 200 μm counter slit. A Siemens Kristalloflex 4 x-ray generator using a Kratky tube with copper target is used to supply x-ray flux. The counts are detected using an LND Xenon filled proportional counter and Siemens preamplifier and Siemens 19" counting panel. Automatic step scanning is carried out by using a Humphrey step Scan 721 with data recorded automatically on a printer. Monochromatization is either by means of a nickel filter and pulse height discrimination or graphite crystal monochromatizer plus pulse height discrimination. The x-ray equipment is housed in a small individually thermostated room to minimize temperature fluctuations.

The intensity data from the sample is corrected for absorption of Cu K_α x-ray in the sample and for long term fluctuations in the x-ray flux from the generator.

The intensity of the instrumental scattering with respect to the sample scattering is also shown in Figure 11. The scattered intensity shown was obtained for sample T-1. In all cases instrumental scattering is equal to or less than sample scattering.

The scattering data is obtained for each range of scattering angles by multiple scans. Each scan over the range of angles consumes 2-3 hours and scans are repeated until at least 5,000 - 10,000 counts are collected for each point in the sample and instrumental scattering scan and at least 3,000 - 8,000 counts are obtained for each point in the instrumental scattering determination. The total time needed for each

of the two scans needed to obtain sample scattering for each of the four ranges of scattering angles is given in Table 5 for sample T-1.

The use of multiple scans reduces the effect of long term variations of x-ray flux on the scattering data. In addition, the total number of counts (or total time to collect a fixed number of counts) can be summed for a given scan and compared to the corresponding sums for preceding and following scans. The deviation of sums from the mean never exceeded 6% with a standard deviation (for sample T-1) of 2.3% in the range $m = .041 \text{ mm} - 0.136 \text{ mm}$, of 2.0% in the range $m = 0.08 \text{ mm} - 0.22 \text{ mm}$, of 1.1% in the range $m = 0.17 \text{ mm} - 0.43 \text{ mm}$ and of 1.7% in the range $m = 0.33 \text{ mm} - 7.11 \text{ mm}$.

Registration of SAXS data at extremely small displacements from the incident beam also requires that the angular displacement at which data is obtained be accurately known and reproducible. The need for this is made clear by Figure 4 in which the incident beam profile obtained using a $15 \text{ }\mu\text{m}$ entrance slit and $30 \text{ }\mu\text{m}$ counter slit is shown together with instrumental scattering beginning with a displacement from the incident beam centroid of $50 \text{ }\mu\text{m}$. It is clear that an error of $5 \text{ }\mu\text{m}$ in the placement of the counter slit can result in an error of 50% in the intensity of scattering for a given value of m . Thus the standard deviation of 2.3% for repeated scan in the smallest range of scattering angles for sample T-1 indicates not only good long term stability of the x-ray source but also good precision in placing the counter slit at exactly the indicated displacement from the incident beam centroid.

Since repeated scans were demonstrated to be reproducible, the following protocol was followed to obtain sample scattering data for the two smallest ranges of angles. Several scans were first made of instru-

Table 5.

Duration of Data Collection for Sample T-1

Range	Sample + Instrumental Scattering (Hours)	Instrumental Scattering (Hours)
1	20	23
2	34	22
3	40	24
4	42	19

mental scattering; the sample was then introduced and sample plus instrumental scattering data obtained for the required number of scans; finally the sample was removed and registration of instrumental scattering data continued. The equivalence of the data for instrumental scattering before and after sample introduction established that no systematic change had occurred in the location of the counter slit with respect to incident beam centroid during introduction of the sample. However, use of this protocol demonstrated that the required freedom from systematic error by introduction of sample could only be obtained by omitting placement of the sample cover (supplied with the camera) over the sample. The action of removing and replacing the x-ray cover was found to introduce systematic errors equivalent to as great as a 5 μm displacement of the counter slit. A lead x-ray shield which did not need to be moved during introduction and removal of the sample was substituted for the sample cover. Finally, comparison of the instrumental scattering obtained as described above, for each sample, with the master instrumental scattering curve, collected together with the incident beam profile and shown in Figure 2, demonstrated that the nominal displacements (m) from the centroid of the incident beam profile were good to at least ± 0.5 μm for the reported sample scattering.

For the data obtained using the Kratky camera 1 (at the larger scattering angles), where small errors in placement of the counter slit would have only a small effect, the instrumental scattering was obtained separately from the instrumental + sample scattering. One instrumental scattering determination was used for every two determinations of sample + instrumental scattering (two separate samples); multiple scans were used in each case; and the sample cover was employed.

The collection of data at very small angles also required correction of the data for the effect of the breadth of entrance and counter slits. The importance of this correction can be understood with the aid of Figure 4. Ideally the width of the incident beam profile would be small in comparison to the separation between experimentally observed points. It is obvious that this is not the case in Figure 4 with both the breadth of entrance and counter slits contributing to the breadth of the incident beam profile. A profile of finite width is required to obtain observable SAXS intensity data. The effect of this finite breadth can be corrected for, as explained in detail in Section 5.1.1.1 of this report. The procedure is carried out directly on the sample scattering data and reduces the observed scattering by as much as 30% for the smallest angles of a given range of scattering angles to between 3% and negligible correction for the highest angles of any given range. The data plotted in Figure 11 are not corrected for the effects of breadth of incident beam profile and for this reason the sample scattering obtained with a 20 μm entrance slit is higher than that obtained for the same scattering angle using a 15 μm entrance slit.

A monochromator was purchased and employed on Kratky camera 2 during the last half of the two year contract. The monochromator was used at the lowest angles because of the short bremsstrahlung radiation scattering will be concentrated at the smallest angles. The bremsstrahlung radiation of longer wavelength than CuK_{α} is less intense than the shorter wavelength radiation and tends to be efficiently absorbed by sample, air, and windows. The monochromator was also intended to discriminate against fluorescent scattering from epoxy samples containing heavy atoms, either by inclusion in the curing agent or by swelling. An

added benefit of the monochromator was that it allowed registration of the incident beam profile (without reduction of the current and potential drop across the x-ray tube) by decreasing the intensity of the beam with a nickel filter of 0.2 mm thickness. The monochromator then allows only CuK_α radiation and integral fractions of that wavelength to reach the proportional counter, whereas the whole short wavelength spectrum (much of it subject to less attenuation than CuK_α radiation) would reach the counter otherwise. In this way Figure 4 was obtained. Registration of the peak of the profile was also used routinely before every series of sample scans (for the two shorter ranges of scattering angles) to supplement the weak Lupolen standard scattering as a means of monitoring the incident beam flux.

5.2.2.2 Results Obtained for Samples Cast on Frekote Coated Plates

As described in Section 4.1, a release agent must be applied to glass plates on which the epoxy resins are cast, in order to achieve subsequent separation of the cured epoxy from the glass. Most of the samples were prepared using a Frekote 34 agent, some of which remained on the resin surface as indicated by its hazy appearance. Results obtained for these samples are presented here.

Data were corrected for the width of the incident beam, but not for the length of the incident beam. The correlation length, \bar{l}_c , was obtained by Debye method and by the Porod method. The Debye plot is carried out with smeared data using a plot of $(\tilde{I})^{-2/3}$ versus m^2 ; the scattering power is obtained from $\int_0^\infty m \cdot \tilde{I}(m)^* dm$, and the Porod range of inhomogeneity is obtained by plotting $m^3 \tilde{I}(m)^*$ vs. m^2 . In these plots, $\tilde{I}(m)^*$ is the smeared scattering intensity minus a constant term, k_2 , as defined in equation 37.

The results obtained for three series of samples are reported. These are samples prepared as shown in Table 6. The x-ray scattering from three series of samples was measured. These are T-1 through T-7, T-4 through T-10, and Q-1 through Q-8 in Table 6. For the three samples in each series, there is a progressively higher curing temperature as one progresses up the series, with a progressively shorter curing time. For the two T series, the epoxy resin is Araldite 6004 with nadic methyl anhydride (NMA) being used as hardener for the first three T samples and dodecyl succinic anhydride (DDSA) being used as hardener for the second three T samples. Ciba-Geigy PT-810 was used as the resin for the Q samples. This is a resin with 3 epoxy groups per molecule and is shorter, stiffer and better defined than the Araldite 6004 resin. The DDSA hardener differs from the NMA hardener in having a bulky side group.

The x-ray data was obtained as described in Section 5.2.2.1. However for the Q samples, the first data point was at 0.1 mm from the centroid of the main beam profile.

The results are given in Table 7. Good agreement is obtained for the Debye and Porod methods of obtaining the inhomogeneity lengths. There appears to be no universal rule that is obeyed in the changes of inhomogeneity length and, in fact, the changes are relatively small. The expectation that shorter inhomogeneity lengths would be observed with increasing curing temperature, in line with the results of Lüttgert and Bonart,⁸ was not satisfied.

More dramatic changes are obtained for the scattering power which is given as

$$(\Delta\rho)^2 w_1 (1-w_1) \quad (1)$$

Table 6. Preparation of Cured Epoxy Samples for SAXS.

Sample Designation	Resin	Hardener (mole ratio)	Cure Temp. (°C)	Cure Time (hrs.)
T-1	Araldite 6004	NMA (0.95)	80	26
T-13	Araldite	NMA (0.95)	140	12
T-7	Araldite	NMA (0.95)	180	6
T-4	Araldite	DDSA (0.95)	80	26
T-16	Araldite	DDSA (0.95)	140	12
T-10	Araldite	DDSA (0.95)	180	6
Q-1	Ciba-Geigy PT-810	NMA (0.9)	80	26
Q-7	PT-810	NMA (0.9)	130	16
Q-8	PT-810	NMA (0.9)	180	6
Q-3	PT-810	NMA (0.9)	80, 120, 140	18, 4, 4
Q-4	PT-810	NMA (0.6)	80	26

Table 7. Analysis of SAXS Data for Cured Epoxy Samples Prepared as Described in Table VI.

Sample Designation	Debye Length (Å)	Porod Length (Å)	Scattering Power [$\frac{\text{mole-electrons}^2}{\text{cm}^3} \times 10^5$]	Debye Calculated Portion of Scattering Power (%)	$\frac{\sum I(\theta)}{Z}$
T-1	1,300	1,300	7.4	45	283
T-13	1,850	1,650	6.5	64	196
T-7	1,250	1,150	2.3	42	102
T-4	1,700	1,600	8	52	250
T-16	1,300	1,100	3.3	45	155
T-10	1,850	1,700	6.5	57	225
Q-1	730	785	1.6	58	106
Q-7					553
Q-8	750	1,060	9.3	57	441
Q-3					38
Q-4					154

for a two phase system. Here $\Delta\rho$ is the electron density difference between the two phases and W_1 is the volume fraction of one phase, $(1-W_1)$ the volume fraction of the other. The scattering power is therefore a measure of the degree of density inhomogeneity of the sample, which we would ascribe to degree of crosslinking inhomogeneity for cured epoxy resins. It is seen that the scattering power decreases with increasing cure/temperature for the first T series (T-1, T-13, T-7), but increases with cure temperature when the stiffer PT-810 is the epoxy resin (Q series). It appears that more SAXS measurements are required to unravel the observed effects.

In this regard it may be noted that the Porod constant (adjusted to constant sample thickness) increases with increase in scattering power. This Porod constant is given in the last column of Table 7, headed $\sim I \cdot m^3/x$. Here x is the sample thickness. The increase of Porod constant with increasing scattering power is given in Figure 12. It may be noted that the Porod constant can be obtained from only one of the four SAXS scans used to obtain the full set of SAXS data. To resolve the cause of low Porod constant (*i.e.*, large inhomogeneity length or low scattering power) only a few points in the SAXS scan at lowest scattering angle need be added. Data from these two scans, the latter considerably abbreviated, could be used as a rapid indicator of trends in a large series of samples. Key samples could then be picked for complete analysis.

In order to interpret the scattering power obtained, it is useful to think in terms of a two-phase model. For such a model, the scattering power may be expressed

$$\overline{(\rho-\bar{\rho})^2} = (\rho_1-\rho_2)^2 W_1 W_2 \quad (21)$$

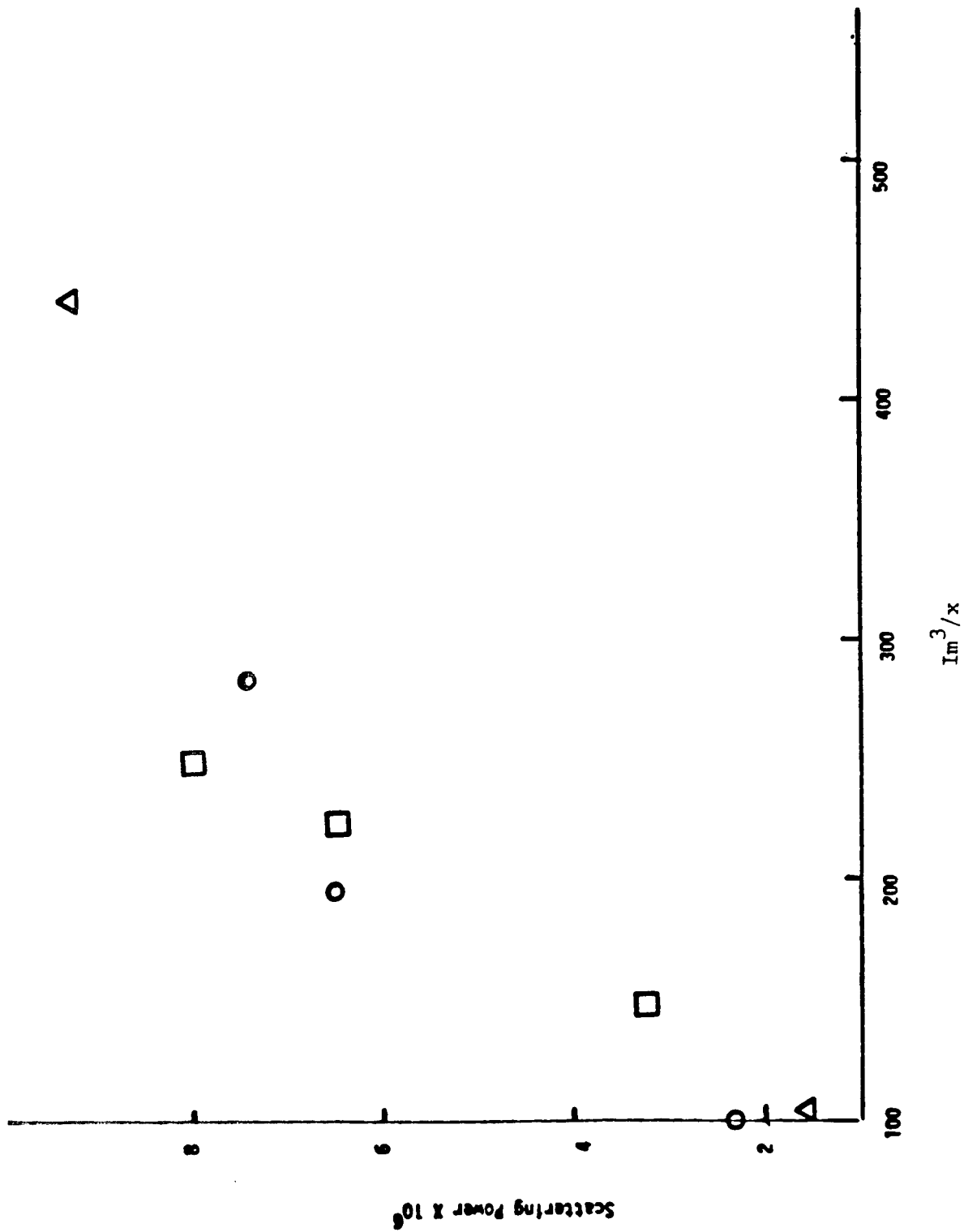


Figure 12. Plot of Scattering Power Versus \tilde{I}_m^3/x (Porod Constant Divided by Sample Thickness).

where ρ_1 , and ρ_2 , are the electron densities of the two phases, and W_1 and W_2 are the respective volume fractions. Thus a scattering power of 5×10^{-6} (mole electrons/cm³)² may be caused by a volume fraction of 2% of a phase differing from the matrix by .02 gms/cm³ or of a volume fraction of 10% of one phase differing from the second phase by 0.01 gms/cm³. By contrast a scattering power of approximately 1.5×10^{-3} [$\frac{\text{mole electrons}^2}{\text{cm}^3}$] has been found for polyethylene by Hermans and Weidinger⁶⁵ and attributed to 80% of a phase differing from the other phase by 0.17 gms/cm³. In converting from mass density to electron density the mass density is multiplied by $\sum Z_i / \sum M_i$ where Z is the atomic number (number of electrons) for each atom in the sample's repeat unit, M is the corresponding atomic weight.

Although the density difference deduced from the scattering powers in Table 7 may appear small, they are compatible with the density difference to be expected between regions differing in degree of cross-linking on the basis of the room temperature density difference between uncured and cured epoxy resin. This has been found to be less than 1% for a typical casting epoxy resin.⁶⁶

5.2.2.3 Results Obtained for Samples Cast on Fluorinated Glow Discharge Polymer Coated Plates

The low scattering power in Table 7, the lack of any consistent trend, and the visual observation for the T-1 through T-7 series that increased scattering power coincided with increased haziness, in combination suggested that the scattering observed for samples cast on Frekote coated glass plates may originate on the surface of the cross-linked resins. In order to ascertain whether the scattering reported in

Table 7 originated in the bulk of the sample, samples T-1 and T-7 were recast on smaller glass plates that had been coated with a fluorinated glow discharge polymer. The glow discharge polymer was deposited in an apparatus employing inductive coupling using a perfluorodidutyltetrahydrofuran monomer with $P_o = 21$ millitorr, $P_g = 50$ millitorr, flow rate $= 0.7 \text{ cm}^3/\text{min}$ (S.T.P.), 62 watts power for 8 minutes. P_o and P_g refer to the pressure before and during the glow discharge respectively. The coating was $1,600 \text{ \AA}$ thick. The infrared spectrum obtained for the glow discharge polymer using the ATR technique and FTIR spectrometer showed one broad band at 1240 cm^{-1} attributed to C-F stretching.

The small angle x-ray scattering in the range $m = 0.05 \text{ mm}$ to $m = 0.43 \text{ mm}$ was considerably smaller for the samples cast on glow discharge polymer than it was for those cast on Frekote. In the range $m = 0.06$ to $m = 0.20$ it was an order of magnitude smaller for sample T-1, approximately 5 times smaller for sample T-7. The scattered x-radiation from the samples was of lower intensity than instrumental scattering up to $m = 0.4 \text{ mm}$ so no quantitative interpretation was attempted. Qualitatively, the small angle scattering for sample T-1 decreased with increasing angle much more precipitously than was the case with T-7. This is the expected result based on Lüttgert and Bonard's theory.⁸

5.2.2.4 X-Ray Scattering From Samples With Varying Crosslink

Density

X-ray scattering investigations were carried out for the series of samples designated, SnDA-3, SnDA-4, etc. as described in Section 4.3, Table 6. In these samples, the crosslink densities were varied by using a primary monoamine (1 hexylamine) in different proportions (to a

diamine) as a chain extender. It was anticipated that some manifestation of the differing intercrosslink distances for the various samples would be found in the x-ray scattering. This has not been the case.

Table 8 shows Bragg spacings obtained from diffuse peaks on WAXS photographs. The Bragg spacings are essentially the same for all samples. They therefore reflect most favorable light atom - light atom distances rather than Sn-Sn distances. The WAXS photographs provide information on Bragg spacings up to 25\AA . Discrete peaks in the SAXS data were sought in the $20\text{\AA} - 300\text{\AA}$ range for SnDA-3 and SnDA-4 and in the $20\text{\AA} - 50\text{\AA}$ range for SnDA-5 with no success.

5.3 Conclusions

An attempt has been made to detect network inhomogeneities in crosslinked epoxy systems by means of small angle x-ray scattering. The SAXS intensity distribution consists of 1) a constant asymptotic value for a portion of the scattering curve, 2) a portion at larger scattering angles where scattering intensity increases gradually with increasing scattering angle and 3) a portion at very small angles where the intensity increases markedly with decreasing scattering angle. Portion 1 of the scattering curve is ascribed to density fluctuations within regions of relatively constant density in the material and is a constant term independent of scattering angle. Portion 2 is the tail of the wide-angle x-ray scattering. Portion 3 has been found in many studies of amorphous systems in general and of epoxy systems in particular and is ascribed to heterogeneities in the system. Although this portion was of very low scattering power, it was chosen for further study because the low room temperature density difference between cured and uncured epoxy systems would be consistent with a scattering curve of such low scattering

Table 8. Bragg Spacings for Peaks in WAXS Photographs (Å).

Sample Designation	Inner Ring	Outer Ring
SnDA-3	18	5.3
SnDA-4	17	5.1
SnDA-5	17	4.9
SnDA-6	17	5.1

power caused by nodules of highly crosslinked resin in a less highly crosslinked matrix. No systematic variation of scattering power or correlation distance (derived from an analysis of portion 3 of the scattering curve) was found with increasing curing temperature for three cured epoxy systems. Portion 3 appears to be associated with residue of release agent left on the surface of the epoxy films after separation from the glass plates between which curing was carried out. A method of coating such glass plates with a thin film of plasma polymer was developed such that portion 3 of the scattering curve is greatly reduced for the resultant cured epoxy films.

The development of a method for making films without SAXS originating at the surface and of methods of collecting and interpreting data at very small angles is a necessary prerequisite for examination of systems in which density differences between highly cured and less highly cured regions are enhanced, e.g., by swelling or by raising the temperature of the SAXS measurement to the curing temperature. Examination of such systems by the SAXS technique may provide the desired indicator of network inhomogeneities.

In order to obtain information concerning the spatial elucidation of crosslinks, epoxy networks were synthesized with varying proportions of S_n containing diamine (providing a heavy atom labeled crosslink) and a monoamine chain extender. No peak, ascribable to heavy atom-heavy atom interactions was found in the SAXS or wide angle x-ray scattering pattern, apparently because of the very broad distribution of crosslink to crosslink distances.

References

1. W. Funke, *Chimia*, 22, 111 (1968).
2. W. Funke, W. Beer, and U. Seitz, *Progr. Colloid. & Polymer Sci.*, 57, 48 (1975).
3. K. Dusek, *Polymer Letters*, 3, 209 (1965).
4. K. Dusek, *J. Polymer Sci.*, C16, 1289 (1967).
5. T. G. Fox and S. Loshaek, *J. Am. Chem. Soc.*, 75, 3544 (1953).
6. W. Fisch, W. Hofmann, and R. Schmid, *Chimia*, 22, 108 (1968).
7. K. Dusek, J. Plestil, F. Lednicky, and S. Lunak, *Polymer*, 19, 393 (1978).
8. K. E. Lüttgert and R. Bonart, *Prog. Colloid. and Polymer Sci.*, 64, 38 (1978).
9. A. S. Kenyon and L. E. Nielson, *J. Macromol Sci.*, A3, 275 (1969).
10. W. Funke, *J. Polymer Sci.*, C16, 1497 (1967).
11. F. Lohse, R. Schmid, H. Batzer and W. Fisch, *British Polymer J.*, 1, 110 (1969).
12. E. H. Erath and R. A. Spurr, *J. Polymer Sci.*, 35, 391 (1959).
13. E. H. Erath and M. Robinson, *J. Polymer Sci.*, C3, 65 (1963).
14. V. Ye. Basin, L. M. Korsunskii, O. Yu. Shokalskaya, and N. V. Aleksandrov, *Polymer Sci. USSR*, 14, 2339 (1972).
15. R. E. Cuthrell, *J. Appl. Polymer Sci.*, 11, 949 (1967).
16. K. Selby and L. E. Miller, *J. Material Sci.*, 10, 12 (1975).
17. J. L. Racich and J. A. Koutsky, *J. Appl. Polymer Sci.*, 20, 2111 (1976).
18. R. Schmid, *Progr. Colloid & Polymer Sci.*, 64, 17 (1978).
19. R. M. Kessenikh, L. A. Korshunova, and A. V. Petrov, *Polymer Sci. USSR*, 14, 466 (1972).

20. H. F. Wohnsiedler, J. Polymer Sci., C3, 77 (1963).
21. L. A. Sukhareva, Yu. P. Kovrizhnykh, and P. I. Zubov, Polymer Sci. USSR, 11, 2147 (1969).
22. T. E. Lipatova, V. K. Ivashchenko, and L. I. Bezruk, Polymer Sci. USSR, 13, 1913 (1971).
23. N. N. Kiryukhin, A. M. Ogrel, A. F. Puchkov, and A. P. Khardin, Polymer Sci. USSR, 13, 2152 (1971).
24. J. L. Racich and J. A. Koutsky, ACS Coatings and Plastics Preprts., 3612, 695 (1976).
25. J. L. Kardos, N. Y. Acad. Sci., 35, 136 (1973).
26. R. J. Morgan and J. E. O'Neal, ACS Coatings and Plastics Preprts., 3G/2, 689 (1976).
27. O. Kratky, G. Porod and Z. Skala, Acta Phys. Austriaca, 13, 76 (1960).
28. A. Belkebir-Mrani, G. Beinert, J. Herz, and A. Mathis, European Polymer J., 12, 243 (1976).
29. J. E. Herz, P. Rempp, and W. Borchard, Adv. High Polymer, 26, 105 (1978).
30. H. Benoit, et al., J. Polymer Sci., Phys. Ed., 14, 2119 (1976).
31. W. Fisch and W. Hofmann, Makromol. Chem., 44/46, 8 (1961).
32. Y. Tanaka and M. Kakiuchi, J. Appl. Polymer Sci., 7, 1951 (1963).
33. R. F. Fischer, J. Polymer Sci., 44, 155 (1960).
34. K. Dusek, M. Bleha and S. Lunak, J. Polymer Sci., Chem. Ed., 15, 2393 (1977).
35. V. F. Kucherov, A. L. Shabanov, and A. S. Onishchenko, Chem. Abst., 59:7381 h.

36. R. S. Wilder and G. D. Martin, U. S. Pat. 2,550,744, Chem. Abst. 46: 2574 g.
37. G. T. M. VanderKerk, J. G. Noltes and J. G. A. Luijten, J. Appl. Chem., 1, 366 (1957).
38. G. H. Reifenberg and W. J. Considine, J. Orgmet. Chem., 9, 505 (1967).
39. W. P. Neumann, H. Niermann and R. Sommer, Am. Chem., 659, 27 (1962).
40. G. Smith, U. S. Pat. 3,332,970.
41. A. Guinier & G. Fournet, J. Phys. Rad., 8, 345 (1947).
42. A. Guinier & G. Fournet, "Small Angle Scattering of X-rays", J. Wiley & Son, N. Y., 1955 p. 116.
43. J. M. W. du Mond, Phys. Rev., 72, 83(1947).
44. V. Gerold, Acta Crystallogr., 10, 287 (1957).
45. S. Heine and J. Roppert, Acta Physica Austriaca, 15, 148 (1962).
46. S. Heine, Acta Physica Austriaca, 16, 144 (1963).
47. R. G. Stanton and W. D. Hoskins, "Numerical Analysis", in "Physical Chemistry", D. Henderson, Ed., Vol., XIA, Academic Press, N.Y., 1975.
48. A. C. R. Newbery, "Numerical Analysis", in "Handbook of Applied Mathematics", C. E. Pearson, Ed., Van Nostrand Reinhold, N.Y., 49. 1974.
49. L. E. Alexander, X-Ray Diffraction Methods in Polymer Science, Wiley Interscience, N. Y. (1969).
50. P. Debye, Am. Physik, 46, 809 (1915).
51. A. Guinier & G. Fournet, "Small Angle Scattering of X-Rays" (translated by C. B. Walker), J. Wiley & Sons, Inc., N.Y. (1955) p. 24.

52. Ibid, p. 127
53. Ibid, p. 149
54. Ibid, p. 70
55. O. Kratky and K. Schwarzkopf-Schier, Monatsch. Chem., 94, 714 (1963).
56. O. Kratky, I. Pilz and P. J. Schmitz, J. Colloid Interfoc. Sci., 21, 24 (1966).
57. G. Porod, Kolloid-Z., 124, 83 (1951).
58. P. Debye, H. R. Anderson, H. Brumberger, J. Appl. Phys., 28, 679 (1957).
59. V. Luzzati, J. Witz and A. Nicolaieff, J. Mol. Biol., 3, 367 (1961).
60. W. Ruland, J. Appl. Crystl, 4, 70 (1971).
61. D. S. Brown, F. P. Warner and R. E. Wetton, Polymer 13, 575 (1972).
62. G. W. Grady, R. Salovey, J. Am. Chem. Soc., 86, 3499 (1964).
63. G. W. Grady, R. Salovey, J. M. Reddy, Biopol., 3, 573 (1965).
64. H. Li, B. Post, H. Morawetz, Makromol. Chem., 154, 89 (1972).
65. P. H. Hermans and A. Weidinger, Makromol. Chem., 39, 67 (1960).
66. H. Lee and K. Neville, Handbook of Epoxy Resins, McGraw-Hill, New York, Chapter 17, 1967.